CHALMERS

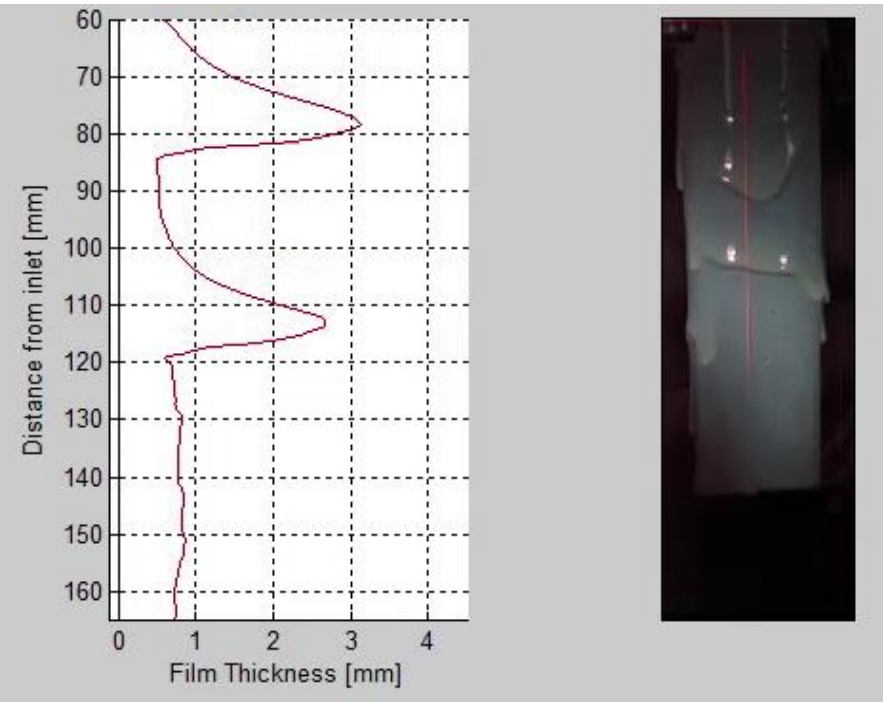

Experimental and Statistical Investigation of Hydrodynamics of a Falling Liquid Film

Master's Thesis within the double Master programme "Energietechnik (University of Stuttgart) – Sustainable Energy Systems (Chalmers University of technology, Sweden)"

CHRISTOPH KARL AMBROS

Department of Energy and Environment
Division of Industrial Energy Systems and Technologies
CHALMERS UNIVERSITY OF TECHNOLOGY
Göteborg, Sweden 2015

MASTER'S THESIS

Experimental and Statistical Investigation of Hydrodynamics of a Falling Liquid Film

Master's Thesis within the *double Master programme "Energietechnik (University of Stuttgart) – Sustainable Energy Systems (Chalmers University of technology, Sweden)"*

CHRISTOPH KARL AMBROS

SUPERVISOR:

Anders Åkesjö

Mathias Gourdon

EXAMINER

Mathias Gourdon

Department of Energy and Environment

Division of Industrial Energy Systems and Technologies

CHALMERS UNIVERSITY OF TECHNOLOGY

Göteborg, Sweden 2015

Experimental and Statistical Investigation of Hydrodynamics of a Falling Liquid Film

Master's Thesis within the *double Master programme "Energietechnik (University of Stuttgart) – Sustainable Energy Systems (Chalmers University of technology, Sweden)"*

CHRISTOPH KARL AMBROS

Department of Energy and Environment
Division of Industrial Energy Systems and Technologies
Chalmers University of Technology
SE-412 96 Göteborg
Sweden
Telephone: + 46 (0)31-772 1000

Cover:
Laser measurement of the film thickness together with a simultaneously taken high-speed image. The laser device can measure the film thickness continuously along the red line with a sampling frequency of 500 Hz.

Chalmers Reproservice
Göteborg, Sweden 2015

Experimental and Statistical Investigation of Hydrodynamics of a Falling Liquid Film

Master's Thesis in the *double Master programme "Energietechnik (University of Stuttgart) – Sustainable Energy Systems (Chalmers University of technology, Sweden)"*

CHRISTOPH KARL AMBROS
Department of Energy and Environment
Division of Industrial Energy Systems and Technologies
Chalmers University of Technology

ABSTRACT

In falling film evaporators a liquid flows down a heated surface as a thin film under gravity. They can be operated at very low pressures and are thus convenient for the evaporation of viscous and temperature sensitive liquids. Falling liquid films are random in nature and the film response is stochastic. The hydrodynamics haven´t been fully understood so far. Therefore the liquid flow pattern are described by statistical analysis.

The flow pattern are investigated at four positions on the outside of a vertical pipe with five meter in length. The dependence on the Reynolds number and viscosity is studied at single positions as well as longitudinal. The experiments are done under non-evaporating- and ambient conditions. The instantaneous film thickness measurements are done by a new laser measurement approach, measuring with a frequency of 500 Hz. A selection of the most promising parameters and statistical methods to describe the liquid flow pattern are determined. A new method has been developed to distinguish between waves with different amplitudes.

The results of the liquid flow pattern by using the new measurement approach results in highly resolved film thickness traces. The new method to distinguish between the waves, gives very pronounced points of transition between different flow regimes.

The transitions from the capillary-wavy-laminar into the inertia-wavy-laminar, from the inertia-wavy-laminar into the inertia-wavy-turbulent as well as the transition into fully turbulent flow have been investigated. The results of the critical Reynold numbers, marking the transitions between the flow regimes show a high dependency on the position at the pipe as well as viscosity.

The work makes a valuable contribution to understand the hydrodynamics of a falling liquid film by investigating the liquid flow pattern.

Key words: Falling liquid film, flow pattern, hydrodynamics, statistical analysis

Contents

Preface

I would like to express my gratitude to the following people.

Anders Åkesjö, for the guidance throughout the thesis, help in questions regarding the theory of falling films and Matlab, the introduction and assistance of experiments and for giving feedback on my report.

Mathias Gourdon, for the guidance throughout the thesis, help in questions regarding the theory of falling films, being my examiner and giving feedback on my report.

Damian Vogt for the help regarding the regulations in Stuttgart.

All people at Chalmers` division of Industrial Energy Systems and Technologies, for their friendly working environment.

Last, but not least, my family and friends, for their encouragement and support.

Thank you!

Christoph Ambros, Gothenburg, June 2015

Notations

Roman upper case letters

A	Wave amplitude	[m]
$\bar{A}$	Total mean wave amplitude	[m]
$\bar{A}_L$	Mean wave amplitude of large waves	[m]
CO_2	Carbon dioxide	
H_2O	Water	
L	Length of the copper pipe	[m]
PDF	Probability density function	
Re_{crit}	Critical Reynolds number	[-]
Std_m	Standard deviation of the mean average Film thickness	[m]
$\dot{V}$	Volume flow	[l/h]

Roman lower case letters

c_p	Specific heat	[J/kgK]
d_o	Outer diameter of the copper pipe	[m]
f	Wave frequency	[1/s]
g	Gravitational acceleration	[m/s2]
$\bar{h}$	Total mean film thickness, averaged over time and laser measurement range	[m]
h_{max}	maximum film thickness at the wave crest	[m]
h_{min}	minimum flim thickness at the wave trough in the front of the wave	[m]
$h_{min}^{'}$	minimum flim thickness at the wave trough, back of the wave	[m]
h_s	Substrate film thickness	[m]

k	Conductivity	[W/Km]
u	Wave celerity/velocity	[m/s]
u_{mean}	mean velocity along the falling film	[m/s]
x	Cartesian axis direction	[m]
z	Distance from fluid inception	[m]
$z_i(x)$	Distance between scanner and film surface	[m]
$z_r(x)$	Reference distance between scanner and clean surface	[m]

Greek symbols

Γ	Mass flow rate per unit width	[kg/sm]
μ	Dynamic viscosity	[Pa s] or [mPa s]
ν	Kinematic viscosity	[m²/s]
ρ	Density	[kg/m3]
σ	Surface tension	[N/m]

Dimensionless numbers

Ka	Kapitza number $\equiv \frac{\rho\sigma^3}{\mu^4 g}$	[-]
Pr	Prandtl number $\equiv \frac{c_p\mu}{k}$	[-]
Re	Reynolds number $\equiv \frac{4\Gamma}{\mu} \equiv \frac{4\delta_{film}v_{z,mean}\rho}{\mu}$	[-]

1 Introduction

First the background of falling liquid film evaporation is given. Beginning with their application and advantages also the difficulties in this field especially the lack of knowledge and need for further research is outlined. This is followed by the objectives and concluded by the scope of the thesis, giving a short description of the procedures.

1.1 Background

In falling liquid film evaporators a liquid flows down a heated surface as a thin film under gravity. They can be operated at very low pressures and are thus convenient for the evaporation of viscous and temperature sensitive liquids. They are used in several heat and mass transfer processes to either concentrate a mixture, for example in the food industry (e.g. orange juice or sugar), desalination plants, recovering processes of water-solvent-paint mixtures) or for the evaporation in refinery and chemical plants like the pulp and paper industry. The letter is the dominant type, using evaporators in Sweden (Bandelier, 1997; Aviles, 2007).

The falling film technique provides several advantages: The short contact time between the fluid and the heat transfer surface is a key factor in food processing or polymer devolitization. The thin liquid layer provokes a high heat transfer coefficient, leading to significant improvements as for example of the cycle efficiency in the refrigeration and heat pump applications. The short fluid holdup is important when it comes to the usage of environmentally hazardous fluids (Alhusseini et al., 1998).

Falling film evaporators can be mainly divided into two types (Aviles, 2007):

- Tube bundle evaporators
- Plate heat exchangers (PHE)

Tube bundle evaporators can be mounted vertical or horizontal. In vertical tube evaporators the liquid to be evaporated can flow either inside or outside of the tube, whereas in horizontal tube evaporators the liquid flows outside. The heat is mostly supplied by condensing steam on the other side of the tube.

Plate type evaporators work with the same principle as tube bundle evaporators but have some advantages. They can be easily adjusted by adding or removing plates as well as they are much more compact due to their higher heat transfer surface to volume ratio.

An essential aspect of falling films is their natural instability and randomness, defined by different kind of waves, occurring as surface waves or roll-waves, provoking the occurrence of turbulence. This intensifies the heat transfer as well as the transition from laminar to turbulent flow. Therefore a fundamental understanding of the interaction between wave dynamics and momentum- and heat transfer especially the liquid flow pattern is of interest. To study falling film evaporation, a research evaporator has been built at Chalmers in cooperation with Valmet, a supplier of evaporators for the pulp and paper industry.

A new laser measurement approach, developed at the *Division of Industrial Energy Systems and Technologies* at the *Chalmers University of Technology*, opens up the possibility for studying the flow and wave pattern in a more detailed way, see *Figure 1.1* .

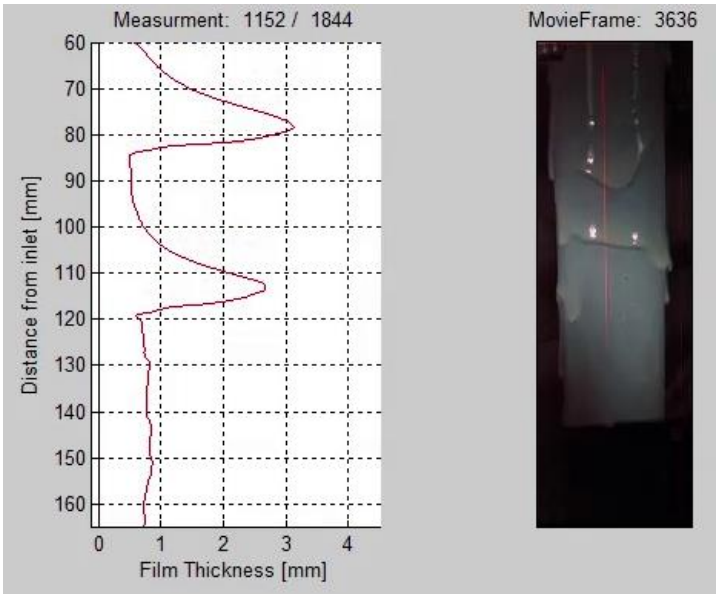

Figure 1.1: shows the laser measurement of the film thickness (left) together with a simultaneously taken high-speed image (right).

It shows the laser measurement of the falling film thickness corresponding to a simultaneously taken high-speed image. The laser device can measure the instantaneous film thickness continuously along the red line with a sampling frequency of 500 Hz. This gives a lot of new information regarding the flow pattern on the tube. The liquid used is a dairy product. The dairy product offers good optical reflection properties which is an essential parameter to gain results with the laser device. Further the viscosity can be changed easily by changing the solid content.

1.2 Objectives

The objective of the thesis is to give a more detailed understanding of the flow phenomena and heat transfer of falling films. The difficulties in describing the mass- heat- and momentum transfer in falling liquid film is the fact, that disturbances acting on the film are random in nature, and the film´s response is stochastic (Telles and Dukler, 1970). The actual state of mathematical tools is insufficient to describe the entire wave system in one complete model. Thus by now the flow pattern, especially the influence of the complex wavy structure on the hydrodynamics is done by identifying statistically meaningful parameters.

With the help of the new laser measurement approach, the influence on the flow pattern and flow state especially the transition- and turbulence regimes can be described statistically using parameters such as film thickness, wave amplitude and its frequency. This gives a more detailed understanding of the flow hydrodynamics and its effect on the heat transfer. Another objective is to investigate the longitudinal flow development by comparing results from one meter pipe to a five meter pipe.

1.3 Scope

For the research evaporator, measurements with the new laser device have already been conducted. The available data are based on experiments with a dairy product. By literature study due to falling films different parameter are investigated to describe the liquid flow pattern especially to distinguish between different flow regimes. Based on this a MATLAB-code is developed, determining these parameters from the recorded measurements.

The flow pattern are described at different locations for different Re as well as dependent on Ka thus viscosity. The existing experimental results are extended with new experiments conducted on a five m pipe. Doing this the longitudinal flow development can be investigated to detect differences between different positions at the tube.

2 Hydrodynamics of Falling Liquid Film

Hydrodynamics is about fluid dynamics and describes how the liquid film flows respectively the flow pattern. For the heat transfer enhancement the understanding of the hydrodynamics is essential as the heat transfer is closely connected to it. Kunugi and Kino, 2005 show in a simulation that local fluctuations in the heat transfer is related to fluctuation of film thickness. Karimi and Kawaji, 1999 investigated the flow characteristics and circulatory motion in wavy falling films with and without counter-current gas flow. They concluded that hydrodynamic mixing, induced by the wavy motion drastically enhance the transfer of momentum, mass and heat across the gas-liquid interface (absorption) and at the wall-liquid boundaries (Karimi and Kawaji, 1999; Adomeit and Renz, 2000).

It is therefore crucial to clarify the influence of interfacial wave characteristics and turbulence structure on the mass and heat transfer. This includes the variation and differences in film thickness, the creation of waves and other hydrodynamic behaviour as dynamic effects as well as the understanding of the different flow regimes and its transitions regions between (Karimi and Kawaji, 1999; Adomeit and Renz, 2000).

Results of experimental observations of a vertical falling film of water and highly viscous fluids show that the flow regimes can be broadly categorized into (Ishigai et al., 1972; Johansson, 2008):

1. *Laminar*
2. First Transition
3. *Wavy-Laminar*
4. Second Transition
5. *Fully Turbulent*

The *Laminar* flow regime is defined as smooth surface, thus no wavy motion on the liquid film respectively negligible rippling. In the *Wavy-Laminar* flow regime pronounced rippling occurs, with surface waves of partially laminar and partially turbulent nature. The *Fully Turbulent* Flow Regime is chaotic and random in nature. The flow becomes shear-flow type, and its wall is identical with that of the turbulent boundary layer (Ishigai et al., 1972; Johansson, 2008).

These regimes are mostly classified by the Reynolds number Re, which describes the ratio of inertial forces to viscous forces, defined as follows:

$$Re = \frac{4\Gamma}{\mu} = \frac{4\delta_{film} u_{mean} \rho}{\mu} \qquad (2.1)$$

Where Γ the mass flow rate per unit circumference is, μ is the dynamic viscosity, δ_{film} is the film thickness, u_{mean} is the mean velocity along the falling film and ρ is the density.

The different flow regimes are sometimes directly conducted due to ranges of Re values. Nevertheless these values cannot be seen as a strict limit as the critical Reynolds numbers Re_{crit}, describing the point of transition between two flow regimes is largely influenced by the surface tension σ. Also gravitational acceleration g and the viscosity μ are dominant forces affecting the falling film flow (Miller and Keyhani, n.d., after 2000). These factors are taken into account by means of dimensionless numbers as

Prandtl number Pr (2.2) and Kapitza number Ka (2.3) (Al-Sibai, 2004; Johansson, 2008).

Chun and Seban 1971 show that Re_{krit} limits decreases with a high Ka number as well as high Pr number. The Pr number is defined as the ratio of kinematic viscosity by the thermal diffusivity and gives information about the relative ease of momentum and energy transport in flow systems (Bird et al., 2007).

$$Pr = \frac{c_p \mu}{k} \qquad (2.2)$$

$$Ka = \frac{\rho \sigma^3}{\mu^4 g} \qquad (2.3)$$

The influence of the Ka number onto the behaviour on laminar wavy films is also shown by Al-Sibai, 2004, who investigated the falling film down a vertical surface. He made a comparison for different falling films which differ in the Re and/or Ka number. The result of Al-Sibai, 2004 are shown in *Figure 2.1*.

With the same Re- but different Ka-numbers between *Figure 2.1 a)* and *Figure 2.1 b)*, there is a clear difference in the manifestation of the waves. A greater similarity can be seen with different Re and Ka numbers between *Figure 2.1 a)* and *Figure 2.1 c)*, although there is a difference in the average film thickness due to the higher viscosity of the fluid in *c)*. This experimental investigation shows that Re is not enough to characterize a falling liquid clearly as the surface tension in the laminar regime is a crucial factor, influencing the liquid flow pattern.

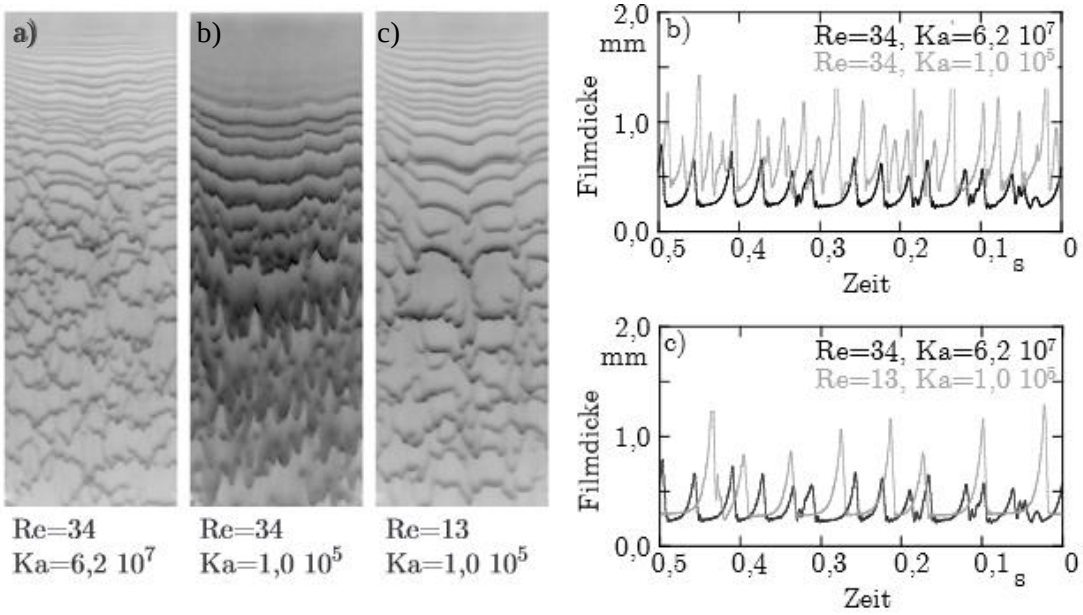

Figure 2.1: Influence of Re - and Ka on the flow characteristics of a falling film. a) Fluorescence image; b) comparison of the flow at the same Re; c) Similar flow at different Re (Al-Sibai, 2004).

In the following subsections, the flow regimes *Laminar*, *Wavy-Laminar* and *Fully Turbulent* are described in more detail as well as influences are given. To be able to clarify the different flow regimes, an overview of the different classes of waves and its properties are presented.

2.1 Laminar Flow Regime

The laminar regime is to be seen as a smooth film without the occurrence of wavy motions. This flow state does almost not occur in the praxis as it only exists for very small Re. Nevertheless Fulford, 1964, Miller and Keyhani, [n.d.] and Al-Sibai, 2004 next to others point that in almost all experiments, there exist a smooth laminar regime/zone near the inlet region, before it transitions into the small-amplitude wavy-laminar flow (first transition). The length of this zone depends among physical factors on the liquid flow rate (described by Re). The smooth laminar film was first studied by Nusselt (1916), who investigated the film thickness over different Re numbers. Later it had been found out that his solution for the film thickness δ_{Nu} only is correct for very small Re numbers. This is for example shown by experiments of Ishigai et al., 1972, who investigated the flow regimes respectively the wavy motion for a water-glycol mixture on the outside of a tube dependent on Re and other physical properties. The film thickness of a purely laminar wavy free flow due to Nusselt only agrees for Re numbers < 4.

As already described the description of the flow regimes is more exact if other physical parameters of the fluid are involved. Thus Ishigai et al., 1972 states an upper limit for the Re number including the Ka number as shown in following equation (2.4) :

$$Re \leq 1{,}88 \cdot Ka^{0{,}1} \text{ (smooth film)} \quad \text{(Ishigai et al., 1972)} \qquad (2.4)$$

Within this range the film is purely laminar free from wavy motion and can be analysed by Nusselt´s laminar theory (Ishigai et al., 1972). Above this value for the Re number the laminar flow regime turns into the wavy-laminar flow regime by passing the first transition region, defined by Ishigai as follows:

$$1{,}88 \cdot Ka^{0{,}1} \leq Re \leq 8{,}8 \cdot Ka^{0{,}1} \text{ (first transition region)} \quad \text{(Ishigai et al., 1972)} \qquad (2.5)$$

Here wavy motions in forms of sinusoidal waves appear, which are highly influenced by surface tension, taken into account by Ka. The wavy motion becomes steady and the maximum film thickness takes a constant value (Ishigai et al., 1972). In this first transition region a first laminar sublayer called the “film substrate” is revealed, identified as the film thickness between the waves. Above this value for the Re number the waves grow in length and amplitude, known as “inertial” or “roll waves” identifying the “wavy-laminar flow regime” (Miller and Keyhani, n.d.).

2.2 Wavy-Laminar Flow Regime

Within the wavy-laminar flow regime small waves already appear at small Re numbers. First sinusoidal waves occur (first transition regime).These are followed by waves with more pronounced amplitude and residuals (Al-Sibai, 2004). The properties of the film substrate in the Wavy-Laminar regime show a partly laminar regime in the substrate and a partly turbulent behaviour in the waves (Ishigai et al., 1972). Fulford, 1964 states that "in thin films a large part of the total film thickness continues to be occupied by the relatively non- turbulent laminar sublayer, even at large flow rates. This is the reason why the transition from the laminar to the turbulent regime cannot be defined sharply by a critical Reynolds number R_{crit} (Fulford, 1964; Miller and Keyhani, n.d.).

Al-Sibai, 2004 pictures this development within an experiment for silicone oil on a inclined flat surface, shown in *Figure 2.2*. The different kind of waves named in the following are especially explained in a subchapter below ("Characteristics/Classification of waves").

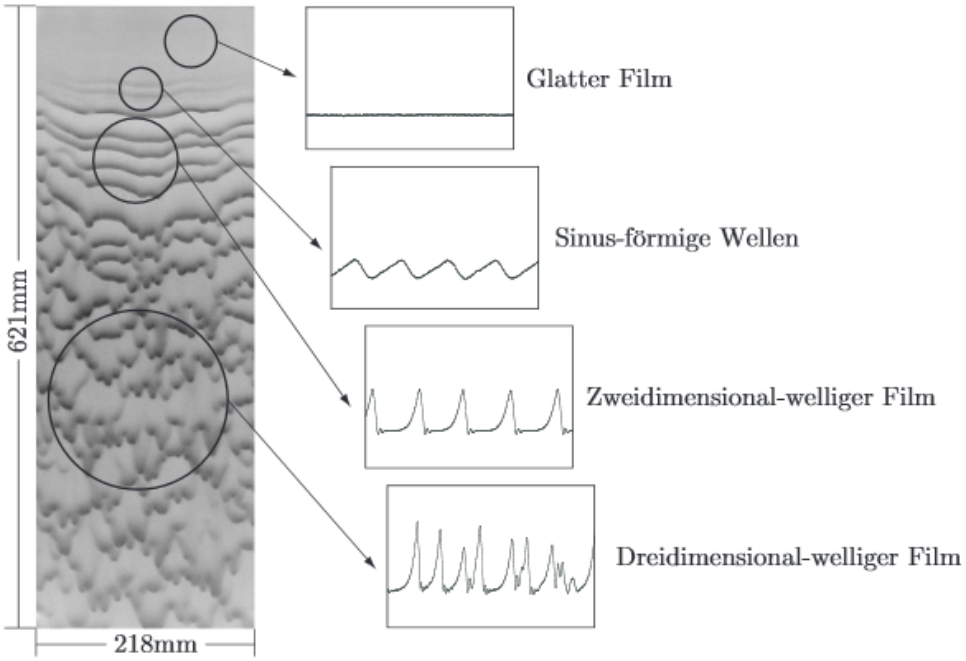

Figure 2.2: Different film contours in the film flow. It is shown the transition from a purely laminar flow (Glatter Film) into a sinusoidal wavy flow (Sinus-förmige Wellen), turning into a two-dimensional wavy flow (Zweidimensional-welliger Film) and finally into a three-dimensional wavy flow (Dreidimensional-welliger Film) (Al-Sibai, 2004).

It is shown that the wave characteristics are greatly dependent upon the longitudinal distance from the liquid entrance (Kil et al., 2001). The surface of the film is only smooth and wave free (laminar) at the beginning of the surface. After this the formation of sinusoidal horizontal waves occurs also known as capillary waves, which in turn transform into horizontal waves with pronounced amplitude (two-dimensional waves) known as inertial or roll waves (Ishigai et al., 1972; Al-Sibai, 2004). (Patnaik and Perez-Blanco, 1996a) and Brauner, 1989 states that the roll waves overtake the smaller capillary waves. Overlapping occurs and the frequency decreases, while the wave velocity, wavelength and amplitude increases.

The two-dimensional waves lose their ringlike symmetry, starting to interfere with adjacent waves resulting in a three-dimensional wave structure, occurring mostly in form of roll waves. The film substrate however still exists (Adomeit and Renz, 2000; Miller and Keyhani, n.d.). The falling film arises as a random array of small and large waves with varying amplitude, length and velocity interacting in a complex fashion (Wasden and Dukler, 1989; Patnaik and Perez-Blanco, 1996; Johansson, 2008(Patnaik and Perez-Blanco, 1996a). This is the stable wavy flow regime which is fully developed (maximum film thickness reaches constant value) (Ishigai et al., 1972; Al-Sibai, 2004).

The stable wavy flow regime is defined by Ishigai as seen in equation (2.6).

$$8{,}8 \cdot Ka^{0{,}1} \leq Re \leq 300 \text{ (stable wavy flow)}, \quad \text{(Ishigai et al., 1972)} \qquad (2.6)$$

With a further increase in the Re number the wavy-laminar flow turns into the turbulent flow. This second transition region is assumed to be within the range of $300 \leq Re \leq 1600$ and independent of physical properties like surface tension σ and viscosity ν (Ishigai et al., 1972). Within this second transition region the type of turbulence gradually changes from the wave-governed to the shear-governed (Ishigai et al., 1972).

Adomeit and Renz, 2000 and Al-Sibai, 2004 agreed with similar results to identify the flow regimes of Ishigai except that of the transition into the fully turbulent regime. Ishigai set the beginning of the fully turbulent regime at a critical Reynolds number Re_{crit} = 1600 independent of Ka. The measurements of Al-Sibai show that the characteristics of the wave amplitude, the standard deviation, the mean film thickness as well as the residual film (substrate) are a function of Ka. Thus the beginning of the fully turbulent regime also has to be defined as a function of Ka, see (2.7) (Al-Sibai, 2004).

$$Re_{crit} = 768 \cdot Ka^{0{,}06} \text{ (beginning of fully turbulent flow)}, \quad \text{(Al-Sibai, 2004)} \qquad (2.7),$$

However the determination of the different flow regimes is very difficult as there isn´t an existing fixed procedure/method. By this different researchers show different values. Next to this also the amount of regimes differ. Ishigai and Al-Sibai for example divide the flow regimes into five including two transition regimes, whereas Patnaik and Perez-Blanco defines the wavy-laminar region as a transition region from laminar to turbulent. The most significant deviations of all values are in the transition to the turbulent flow. *Table 2.1* gives an overview of the values depending on different authors. There it can also be seen that some authors divide the transition between the regimes by a critical Reynolds number Re_{crit} (Brauer, Patnaik and Perez-Blanco) whereas others define a transition region (Ishigai, Al-Sibai). The different authors further uses different definitions of Re. The values in *Table 2.1* therefore have been normalized to the Re defined in equation (2.1).

The effects leading to transition to the turbulence regime are explained in the following subsection, where a deeper insight into the waves is given.

2.2.1 Characteristics/Classification of waves

In the wavy-laminar flow regime the transition to turbulence and surface disturbance become more significant with increasing Re number. This transition can be subdivided into capillary wavy-laminar, inertial wavy-laminar and inertial wavy-turbulent flow regime. Inertia waves are commonly known as "roll waves" because of their appearance of rolling down over the film substrate (Patnaik and Perez-Blanco, 1996; Johansson, 2008). According to Patnaik and Perez-Blanco the transition region correspond approximately to the Re number ranges, $20 < Re < 200$, $200 < Re < 1000$, and $1000 < Re < 4000$, respectively.

In the low Re number range ($20 < Re < 200$) of the capillary-wavy flow, surface tension forces dominates the effect of gravity and thus play a key role in the manifestation of the waves. These waves appear as ripples on the film surface, being of high frequency and small amplitude, also known as sinusoidal traveling waves, seen in *Figure 2.2* (Patnaik and Perez-Blanco, 1996; Johansson, 2008; Dietze et al., 2008). Karimi and Kawaji, 1999 measured the velocity profile and film thickness simultaneously in a vertical tube to better understand the turbulence characteristics and the effect of interfacial waves and shear on the heat and mass transfer rates. They concluded that surface ripples almost have no influence on the near-wall hydrodynamics, while larger waves could be easily sensed close to the solid wall, altering the turbulence intensity profiles.
An important phenomenon influencing the mass transfer in the capillary wavy laminar region is the backflow. This phenomenon was studied in detail by Dietze et al., 2008, and was confirmed by numerical simulation on highly resolved spatial and temporal grids. Dietze was the first to be able to identify and explain, the mechanism leading to the origination of the backflow phenomenon. Later Dietze et al., 2009 confirmed the backflow phenomenon based on experimental studies using laser Doppler velocimetry (LDV) and particle image velocimetry (PIV). The backflow arise as the result of a separation eddy, developing at the bounding wall similar to the case of classical flow separation. The capillary separation eddy (CSE) is induced by a positive pressure gradient in the capillary-wave region as a result of change in curvature of the free surface. The CSE significantly enhances the heat transfer from the bounding wall to the liquid, based on crosswise velocities/convection (Dietze et al., 2008; Dietze et al., 2009). A continuative detailed study on the backflow dynamics is done recently by Doro, 2012.

With a Re number > 200 roll waves appear, governed by the interplay of inertia and gravity, with surface tension effects becoming negligible in comparison. Roll waves have longer wavelengths and much lower frequencies than capillary waves. The waves accelerate and grow downstream reaching amplitudes from two to five times the substrate thickness. As seen in *Figure 2.3* they create their own layer (overlying layer) visualized as rolling liquid lump, transporting the major part of the flow rate by travelling over a slow-moving thin substrate film (underlying layer) (Patnaik and Perez-Blanco, 1996a); Brauner, 1989; Johansson, 2008).

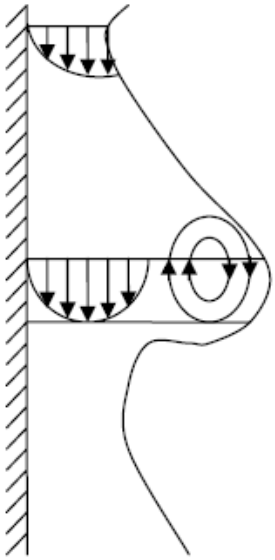

Figure 2.3: Falling film with roll waves, belonging to the wavy laminar flow regime. The profile of the flow is depending on the flow regime. The profile is sketched by Johansson, 2008 *according to the flow profile of* Brauner, 1989

In the wave core a large mixing eddy is formed even at low average film Re numbers, while the substrate film remains laminar. The mixing eddy is considered to be part of turbulent field. With increasing flow rate the turbulence will further extend to the substrate layer. Because of the penetration into the substrate, the slower velocity liquid in the substrate is continuously picked up and mixed into the wave front. This in turn leads to a grow in mass, acceleration down the pipe and causes thinning of the film substrate until it finally results in a fully turbulent flow field (Johansson, 2008; Miller and Keyhani, n.d.). Chu and Dukler, 1974 observed the mass flow rate in the roll wave which resulted in a 10 to 20 times higher value than in the substrate. Different authors revealed the occurrence of circulatory motions with significant velocities normal to the tube wall under large waves. They concluded that this can explain the dominant mechanism of enhanced rates of heat and mass transfer observed in wavy film flow (Brauner, 1989; Karimi and Kawaji, 1999; Patnaik and Perez-Blanco, 1996a; Wasden and Dukler, 1989). Thus the main role of the recirculating eddy lies in triggering the initiation of turbulence (Brauner, 1989; Johansson, 2008). Although the wavelength of the roll waves is large enough to make capillary effects negligible over most of the wave, the amplitude and curvature of the steep front is sufficiently great to lead to the formation of capillary ripples at the toe of the main wave (Fulford, 1964).

Table 2.1: Different Re numbers for the classification of flow regimes

Regime	Brauer 1956 reported by Weise and Scholl, 2007	Ishigai et al., 1972	(Patnaik and Perez-Blanco, 1996a)	Al-Sibai, 2004
Laminar	$Re < 16$	$Re \leq 1.88 \cdot Ka^{0,06}$	$Re \leq 20$	$Re \leq 2.4 \cdot Ka^{0,06}$
Wavy laminar	$16 \leq Re \leq 1600$	$8{,}8 \cdot Ka^{0,1} \leq Re \leq 300$	$20 < Re < 4000$	$Re \leq 128 \cdot Ka^{0,1}$
Fully turbulent	$Re \geq 1600$	$Re \geq 1600$	$Re \geq 4000$	$Re \leq 768 \cdot Ka^{0,06}$

In conclusion it can be said that two classes of waves are typically identified. The first are ripple waves with small amplitudes, covering the substrate and decay quickly after their inception. The second waves are disturbance waves. They carry a significant amount of the liquid, with amplitudes typically a factor of up to five times the substrate film thickness. Their influence can be sensed closed to the wall hydrodynamics and are known for initiating turbulence. However the wave type nomenclature remains unsettled and the definitions of the two main wave types are not without some ambiguity. As a result, a clear distinction between the different wave types is still lacking, which, consequently, can lead to discrepancies in the definitions and distinctions between the different flow regimes (Chu and Dukler, 1974, 1975; Zadrazil et al., 2014).

2.3 Fully turbulent Flow Regime

Turbulent flow is defined by its randomness, is rotational and three-dimensional. They are always dissipative. "The diffusivity of turbulence causes rapid mixing and increases rates of momentum, heat, and mass transfer"(Johansson, 2008)."Viscous shear stresses perform deformation work which increases the internal energy of the fluid at the expense of kinetic energy of the turbulence"(Johansson, 2008).

The interfacial instability result in the onset of small interfacial ripples, developing downstream into highly disturbed lumps of liquid, the rolling waves. These large waves building their own layer traveling over the substrate film and cause an increase in the transport rates of momentum heat and mass across the liquid film (Brauner, 1987; Fulford, 1964). According to Ishigai et al., 1972 the beginning of fully turbulent flow can be recognized by the decay of the wave crest. Brauner, 1989 points out, that turbulence may first be initiated in the wave core as mixing eddies. He modelled the wavy flow in turbulent falling films and concluded that the transition to turbulence is controlled by the local instantaneous Re. The local Re is a random process as the local flow rate varies with the local film thickness (Chu and Dukler, 1974). This Re is expected to attain a transitional value first in the wave back region. Thus intermittent turbulence may be commenced in the flow field already at relatively low overall Re, with turbulence prevailing in the wave back region, while the thin film substrate remains still laminar. However, with increasing flow rate the turbulence also develop in the wave trail region and further extend to the film substrate film with increasing flow rate (Brauner, 1987, 1989).

Turbulent films consist of three regions: a viscous boundary layer close to the wall, a turbulent core and a viscous boundary layer near the free interface (Alhusseini and Chen, 2000).

In usual pipe flows, the turbulence is initiated near the wall in form of bursts, generating large eddies. The larger eddies transfer the turbulence to the smaller eddies and eventually dissipated by a viscous mechanism. In falling films however the eddy size is limited by the thickness, usually very small. In addition, the film surface has two competing effects on turbulence, depending on the surface waves. The smooth surface tends to damp out any abrupt turbulences generated at the wall (wall turbulence). The wavy surface however, cause fluctuations in film thickness and surface as well as stream-wise liquid velocities. This is regarded as wave-induced turbulence. The extent of these mechanism depends on the wave amplitude as well as on other factors, such as Re, physical properties and geometry. Hence, with these inherent characteristics, turbulence is difficult to be initiated and sustained in smooth films at small Re. But, once the film becomes wavy and turbulent, the turbulence intensity distributions are amplified and generally greater than those of single-phase pipe flow (Karimi and Kawaji, 1999).

3 Methods to investigate Liquid Flow Patterns

Measurements methods to investigate the wavy motion of a falling liquid film have been conducted since 1950´s. Examples for this are: the electrical resistance method, the capacitance method, the light-absorption method, the light-reflexion method (Ishigai et al., 1972), needle contact probe (Takahama and Kato, 1980), electric capacity method (Takahama and Kato, 1980), parallel-wire conductance (Drosos et al., 2004) technique and shadow photographs (Al-Sibai, 2004).

More recently Patnaik and Perez-Blanco, 1996 observed the velocity field of inertial/roll waves by an image-processing system. They especially investigated the velocity field of roll waves as well as applied a frequency analysis. An outcome of the study is the relationship between wave parameters and flow parameters.

Karimi and Kawaji, 1999 measured the instantaneous velocity profiles in the wavy falling liquid films by using a photochromic dye tracer technique, based on a reaction of a photochromic dye material dissolved in the liquid with a high intensity ultraviolet laser beam. The motions of traces formed were recorded using a high speed CCD camera. The velocity profile was measured simultaneously with the film thickness to better understand the turbulence characteristics and the enhancement effect of interfacial waves and shear on the heat and mass transfer rates.

Adomeit and Renz, 2000 investigated the flow and surface structure in laminar wavy films and measured the velocity distribution by particle image velocimetry (PIV) and film thickness by a fluorescence technique. Doing this they gained detailed information on the transient conditions within the three-dimensional wavy flow. The PIV was chosen as it is able to measure the instantaneous velocity field and thus is significantly better suited for the application to a transient flow compared to spatially discrete measurement systems such as LDA.

Dietze et al., 2008 investigated the backflow in falling liquid films experimentally and by numerical simulation. He applied the laser-Doppler velocimetry (LDV) and a confocal chromatic imaging method, to measure the instantaneous local streamwise velocity and film thickness simultaneously.

A comprehensive overview as well as the development of different techniques to investigate parameters of liquid flow pattern starting from the 1910´s till 2005 is given by Al-Sibai, 2004. Also Aviles, 2007 gives an overview about available methods for the measurement of the film thickness. He specialized on methods and their possible application for the special case of evaporation on structured heating surfaces.

Most of the developed methods are used to measure the average film thickness. For the measurement of the local film thickness, different methods have been developed, but only a few were able to measure the wavy film temporally and spatially highly resolved as they disturb the flow directly or indirectly (Al-Sibai, 2004). The local film thickness is a crucial factor as it results in significant parameters to describe the flow characteristics. Salazar and Marschall, 1978 measured the local thickness and their results indicated clearly the importance of measurement location on film characteristics.

In addition, most of the methods are only able to determine an average film thickness and some to determine a thickness in a single point (Akesjö et al., 2015). Information about the behaviour of the flow over a distance is rarely given. The turbulence regime in falling films is not well understood because of a lack of data on the structure of

turbulence. Experimental investigations have been hampered by the difficulties associated with the probing of thin films (typically of thickness less than 1mm) without interference by, or disruption to, the wavy interface (Alhusseini and Chen, 2000).

A new measurement approach, consisting of a laser triangulation scanner bridges this gap. The laser device can measures the film thickness along a vertical line in 1280 points with a sampling frequency of 500 Hz. This resolves the flow pattern in high detail without influencing it (Akesjö et al., 2015). More information about the laser device is given in Chapter 5, where the test facility respectively the experimental setup is explained.

4 Statistically Data Analysis

The difficulties in describing the mass- heat- and momentum transfer in falling liquid films are, that disturbances acting on the film are random in nature, and the film´s response is stochastic (Telles and Dukler, 1970). The actual state of mathematical tools is insufficient to describe the entire wave system in one complete model. Thus the target is to describe the flow pattern, especially the influence of the complex wavy structure on the hydrodynamics by identifying statistically meaningful parameters.

The first time-resolved method to investigate liquid flow pattern was done by Dukler and Berglin 1952. Later, an attempt was made to expand the knowledge about falling film flow through statistical analysis of wave characteristics. Particularly noteworthy are the studies of Telles and Dukler, 1970, Chu and Dukler, 1974, Chu and Dukler, 1975, Salazar and Marschall, 1978 and Brauner and Maron, 1982. The methods developed by them are applied in a range of studies as for example by Al-Sibai, 2004, (Drosos et al., 2004) and Aviles, 2007, between others.

Telles and Dukler, 1970 investigated the surface structure on a liquid film, shear driven by a gas flow. They applied the electrical conductivity method to track the film thickness fluctuations. Statistical methods, namely the auto- and cross-correlation of the film thicknesses in the frequency domain were implemented to obtain the average velocity and frequency of the waves. They further determined the separation distance between the waves, wave amplitude and shape.

Chu and Dukler, 1974 further improved these methods and compared them to predictions of theory, developed for mean substrate thickness and flow rate. Small wave structures were treated by extracting the statistics of the wavy motion from a series analysis. They concluded that the statistics of the film thickness are greatly influenced by the substrate and its waviness. Two groups of statistical parameters are used: the first considers the film thickness of the substrate as a random process and the second considers the individual small waves on the substrate as a random process. The film thickness probability distribution is used to calculate the thickness of the substrate and that of the waves as well as to determine the fraction of those.

In a subsequent work, Chu and Dukler, 1975 defined the substrate thickness based on a statistical approach using probability density distribution (PDF) of the instantaneous film thickness. They showed that the film has bimodal characteristics consisting of large and small waves. The two groups of statistical parameters especially investigated here, are the film thickness itself as a random process and the individual large waves as a random process. They concluded that large waves dominate the transport characteristics in the film, while small waves control transport characteristics in the gas. Further Chu and Dukler concluded from different experiments, that at any fixed point along a surface the substrate is present for a large fraction of the time and thus plays an important role in mass-, momentum- and heat between the wall and the liquid (Chu and Dukler, 1974).

Salazar and Marschall, 1978 presented results of the time-varying local film thickness with the help of the laser scattering method (suspended particles). For the statistical analysis they used *Jeffreys theory of drainage* to determine the time-average local film thickness. They demonstrated the dependence of local time average film thickness on Re as well as on the measurement location along the direction of the flow.

Brauner and Maron, 1982 provided information about the instantaneous local heat- and mass transfer rates simultaneously to the local instantaneous film thickness by the

electrochemical technique (chemical reduction of ferricyanide ions at a nickel cathode) and the capacitance method respectively. Measurements are done at different points all along the undeveloped as well as the developed regions. For the statistically analysis stochastic techniques, namely sampling and evaluating the power spectral and cross-spectral densities are applied.

Another study Karapantsios et al., 1989 described falling films in terms of various statistical moments of a film thickness (i.e., mean, root-mean-square), probability density functions (PDF) and autocorrelation functions (ACF) of the interfacial film thickness variations. Further the waves were characterized via the evaluation of the power spectral density (PSD) and PDF of the wave peaks.

(Mascarenhas and Mudawar, 2014) investigated the longitudinal flow characteristics of water flowing outside of a vertical tube at different locations between 30-450 mm from the entrance. Statistical methods, namely probability density function, variance, Cross- and Auto-Covariance are employed to examine the evolution of film thickness and interfacial temperature in turbulent, free-falling film.

4.1 Liquid Film Parameter of Interest

Chu and Dukler, 1974, 1975, show that a falling liquid film consists mainly of the film substrate and waves. The *film substrate* also known as *residual film* is identified as the (smooth) regime between the waves. Chu and Dukler, 1974 recognized, that the transport of heat- and mass is influenced by the characteristics of the residual film.

In the statistical analysis they categorized the waves into a two wave system. Large waves (roll waves) carrying the bulk and small waves, existing over the substrate, as well as across the large waves (Telles and Dukler, 1970; Chu and Dukler, 1974). The film substrate lies between the solid wall and the surface waves, as well as represents the zone between the large waves. The latter is often referred to as residual film. The amplitude of all large waves varies with the time and location (Chu and Dukler, 1974;Kostoglou et al., 2010).

Large waves have large fluctuations taking place around the mean film thickness, with the maximum and minimum amplitude associated with the wave being on alternate sides of the mean film thickness. *Small waves* on the substrate appear to be completely below the mean film thickness.

For the statistical analysis of falling liquid films researchers as Telles and Dukler, 1970; Chu and Dukler, 1974-1975; Salazar and Marschall, 1978; Brauner and Maron, 1982 who laid the foundation of the statistical analysis as well as more recently Al-Sibai, 2004; Dietze et al., 2008 and Mascarenhas and Mudawar, 2014 agreed on the same parameter. Seven parameters are used for data processing, divided into the *Time Domain* and *Amplitude Domain*.

In the *Time Domain*, the parameters which are of interest are: time for passage of the base T_b, wave separation time T_s, time for passage of the wave front T_{bf}, and time for passage of the wave back T_{bb}. The separation time T_s differs from the base dimension T_b because of the existence of a wavy substrate between two large waves.

The parameters of interest in the *Amplitude Domain* are wave amplitude A, maximum film thickness at the crest of the wave h_{max} as well as h_{min} and $h_{\acute{m}in}$, representing the

minimum film thickness at the trough of the wave front and back respectively, see *Figure 4.1* (Chu and Dukler, 1975, 1974).

According to these parameters, the falling liquid film can be analyzed statistically respectively the data can be processed.

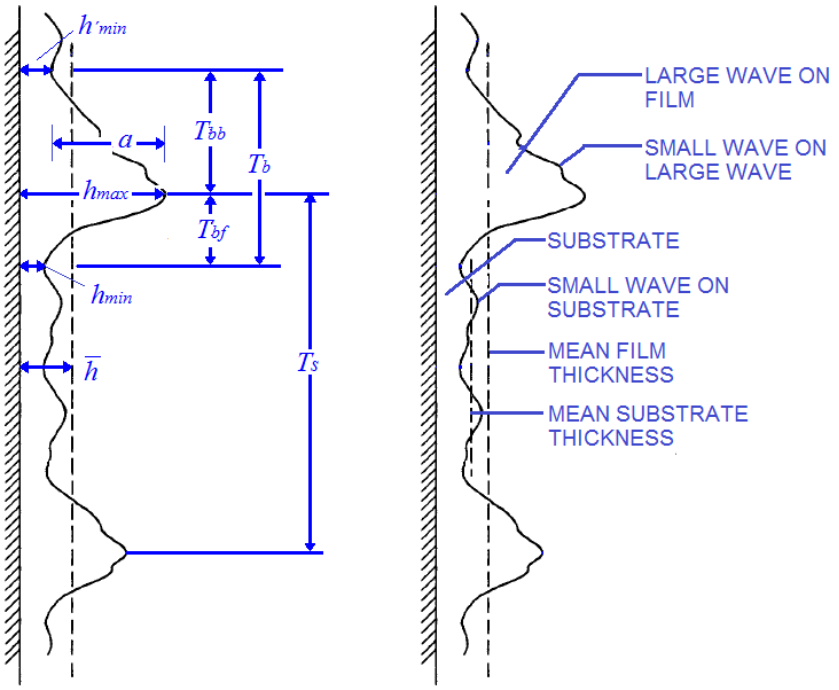

Figure 4.1: wave classification (right) and wave parameter of interest (left) according to Chu and Dukler, 1974.

In order to characterize the waves statistically, the time averaged film thickness $\bar{h}_i$ has to be calculated:

$$\bar{h_i} = \frac{1}{n}\sum_{i=1}^{n} h_i(t) \qquad (4.1)$$

The classes of waves can then be identified as follows (Chu and Dukler, 1974) :

(i) A large wave exists if:

$$h_{max} > \bar{h} \quad \text{and} \quad h_{min}, h_{min}' < \bar{h}$$

(ii) A small wave on the substrate exists if:

$$h_{max}, h_{min}, h_{min}' < \bar{h}$$

(iii) A small wave on a large wave exists if:

$$h_{max} > \bar{h}, \quad h_{min} > \bar{h}, \quad h_{min}' < \bar{h}$$
$$h_{max} > \bar{h}, \quad h_{min} < \bar{h}, \quad h_{min}' > \bar{h}$$
$$h_{max} > \bar{h}, \quad h_{min} > \bar{h}, \quad h_{min}' > \bar{h}$$

where h_{max} is the local maximum at the crest of the wave, h_{min} and $h_{min}^{'}$ are the local minima at the trough in front and in the back of the wave respectively. These maxima and minima are local extrema of the film thickness. Global values for the maxima and minima are used, if not only a single wave is investigated but a film thickness track over time. The local time-averaged liquid film thickness $\overline{h_t}$ is necessary in order to obtain the mean film thickness throughout the whole pipe length $\bar{h}$.

The *wave amplitude* A is an important factor when it comes to determination of flow regimes especially the transition into the fully turbulent flow regime. The beginning of fully turbulent flow can be recognized by the decay of the wave crests. The w*ave amplitude* can be used to illustrate this effect. The amplitude increases with increasing Re-number, reaches a maximum at a certain Re-number and then decreases again (Ishigai et al., 1972; Al-Sibai, 2004). Al-Sibai, 2004 defines the *wave amplitude* a as seen in (4.2) with a maximum film thickness h_{max} and minimum film thickness h_{min}, assuming a constant minimum film thickness in front and in the back of the wave trough. According to Chu and Dukler, 1974 the minimum film thickness in front and back of a wave are not necessarily the same. That's why they defined the *wave amplitude A* with an average in the minimum film thickness, see (4.3).

$$A = h_{max} - h_{min}, \text{(Al-Sibai, 2004)} \qquad (4.2)$$

$$A = h_{max} - \frac{(h_{min} + h_{min}^{'})}{2}, \text{(Chu and Dukler, 1974)} \qquad (4.3)$$

The instantaneous *film thickness* $h(t)$ is a random fluctuating quantity. Thus time series analysis can be applied to provide more statistical parameters such as *probability distribution* $F(h)$ *and probability density function* PDF.

These are defined as follows, (Chu and Dukler, 1975; Karapantsios et al., 1989; Takahama and Kato, 1980; Mascarenhas and Mudawar, 2014):

$$F(h) = Prob\{h(t) < h\} = \frac{n\{h(t) < h\}}{N} \qquad (4.4)$$

$$PDF(h) = \lim_{\Delta h \to 0} \frac{Prob\{h < h(t) < h < \Delta h\}}{\Delta h} = \frac{dF(h)}{dh} \qquad (4.5)$$

The PDF(h) of the variable film thickness h, is the representation of expectation of occurrence of all possible values of that variable, where N is the total number of samples and n the number of samples in a subset of the time recorded. In contrast to the mean film thickness values the probability density provide information about the manner in which these variables are distributed about the mean (Mascarenhas and Mudawar, 2014). With the PDF it is possible to presume the interfacial characteristics of the film by identifying the substrate thickness and wave amplitude. The peak of the PDF corresponds to the most frequent thickness, referred to as the substrate thickness h_s (Mascarenhas and Mudawar, 2014). Also Chu and dukler 1975, Moran et al., 2002 and Al-Sibai, 2004 defined the substrate thickness by evaluating the probability density function PDF of the instantaneous film thickness data.

For the determination of the global *minimum* and *maximum film thickness* a Probability distribution can be generated, where F(h)=1 and F(h)=0 represent the maximum and minimum film thickness respectively. Takahama and Kato, 1980 state that h_{max} increases linearly downstream except in the entrance region where it increases more rapidly. This procedure was also applied by Al-Sibai who further developed this method by determining values with a certain frequency. Using these values instead of the smallest or largest quantity of a measurement the distortion due to interference effects (falling droplets) is minimized.

By introduction of the *variance var* (4.6) and the *standard deviation* Std (4.7), where x represents the measured value, a measure of dispersion of the data about their mean value can be provided (Karapantsios et al., 1989 Drosos et al., 2004).

. $$var = \frac{1}{N-1}\sum_{i=1}^{n}(x_i - \bar{x})^2 \qquad (4.6)$$

$$Std = \sqrt{var} = \sqrt{\frac{1}{N-1}\sum_{i=1}^{n}(x_i - \bar{x})^2} \qquad (4.7)$$

Takahama and Kato, 1980 applied the variance of the film thickness to show the longitudinal distribution of the variance of interfacial waves. He investigated the Re between $200 - 2000$ at 9 different locations between $100 - 1700$ mm outside of a vertical tube. Below an $Re = 1000$ the variance is still small at the entrance region of $z < 500$ mm indicating that large wavy motion does not occur. Further downstream var increases rapidly pointing that waves with larger amplitudes prevail. For a $Re > 1000$ also at a location of 100 mm downstream the entrance, fluctuations corresponding to large waves occur. From all measurements it can be seen that the variance and thus also the standard deviation have a limiting value as the amplification of the wave amplitude has (Takahama and Kato, 1980). The wave amplitude can only grow till a certain maximum, depending on the film thickness h, Ka and Re.

Mascarenhas and Mudawar, 2014 applied the variance on the film thickness for a constant Re at the fluid entrance at 8 locations longitudinal to the pipe. The variance increases appreciable downstream till around 200 mm from fluid inception influenced by the boundary layer development. Further downstream of 200 mm the increases is muted and show a trend towards a constant level indicating fully developed wavy flow.

Al-Sibai applied these values on the wave celerity (4.8). With an increasing Re the variation of u increases, identifying a transition from the stable wavy-laminar flow into a regime where the collision and interaction of waves leads to inhomogeneous velocities and local turbulences (Al-Sibai, 2004).

The *wave celerity* (wave velocity) is determined as an averaged value between two measurement points according to:

$$\bar{u} = \frac{\Delta z}{\Delta t} \qquad (4.8)$$

where Δz and Δt represents the distance between the measurement points and the time the wave needs to travel in between respectively. The wave celerity mustn't be interpreted as the transport velocity, as the proportion of the interchanged fluid volume

is unknown and depends on many factors. Further the wave celerity it is not to be confused with the surface speed of a film. Falling films can consist of more than one typical wave celerity. The celerity as well as the width of the celerity spectrum increases with increasing Re number (Karapantsios et al., 1989; Drosos et al., 2004).

Paras and Karabelas, 1991 as well as Drosos et al., 2004 determined the wave celerity by signal cross-correlating of two fluctuation film thickness signals recorded simultaneously between two neighbourly locations. The wave celerity (4.8) is calculated by determining the time delay between two successive peaks. The wave celerity increases with Re as well as downstream attributed to an increase in wave amplification (Drosos et al., 2004; Paras and Karabelas, 1991).

The *Wave Frequency* is an essential parameter to characterize the wave type. In the falling film many frequencies are present but the one of a single frequency could be dominant (that of the roll waves) and most instrumental in transport enhancement (Patnaik and Perez-Blanco, 1996a). For the determination of the frequency, (Patnaik and Perez-Blanco, 1996a) and Al-Sibai, 2004 used the Fourier-Transformation in which a signal is broken down into the sum of individual sin waves and converted from the time to the frequency domain. The most common frequency is referred to as *wave frequency* (Patnaik and Perez-Blanco, 1996; Al-Sibai, 2004).

5 Test facility

In this Chapter first the experimental setup of the test facility is explained. This is followed by a more detailed investigation of the laser measurement device, it´s calibration as well as validation of the results.

5.1 Experimental setup

A schematic sketch of the test facility including the main parts of the periphery is shown in *Figure 5.1*. The distributor is mounted on top of the tube. The experiment has been investigated on two tubes due to limitations of the laser measurement system. Both tubes have the same outer diameter d_o= 60 mm but are different in length. Throughout the thesis the distances are referred to the point of fluid inception, which is defined as $z = 0$. This is the bottom point at which the distributor is connected to the pipe. The real point of fluid inception is 250 mm above ($z = -250\ mm$). The experiments done at distances of 30 mm and 450 mm are investigated on a copper pipe with 0,8 m length. The distances at 2 m and 4,5 m have been investigated on a 5 m steel pipe.

The surface roughness of the pipes may differ but the influence is assumed to be negligible on the flow pattern of the falling film. The distributor guarantees an even distributed liquid film, flowing on the outside of the tube. The falling film visualization is achieved by the Laser Scanner. The pump (Circ.pump) maintain a fixed circulating flow. Flow rate, density, viscosity and temperature are measured online. The quantity and accuracy of the measurement instruments can be seen in *Table 5.1* (Akesjö et al., 2015).

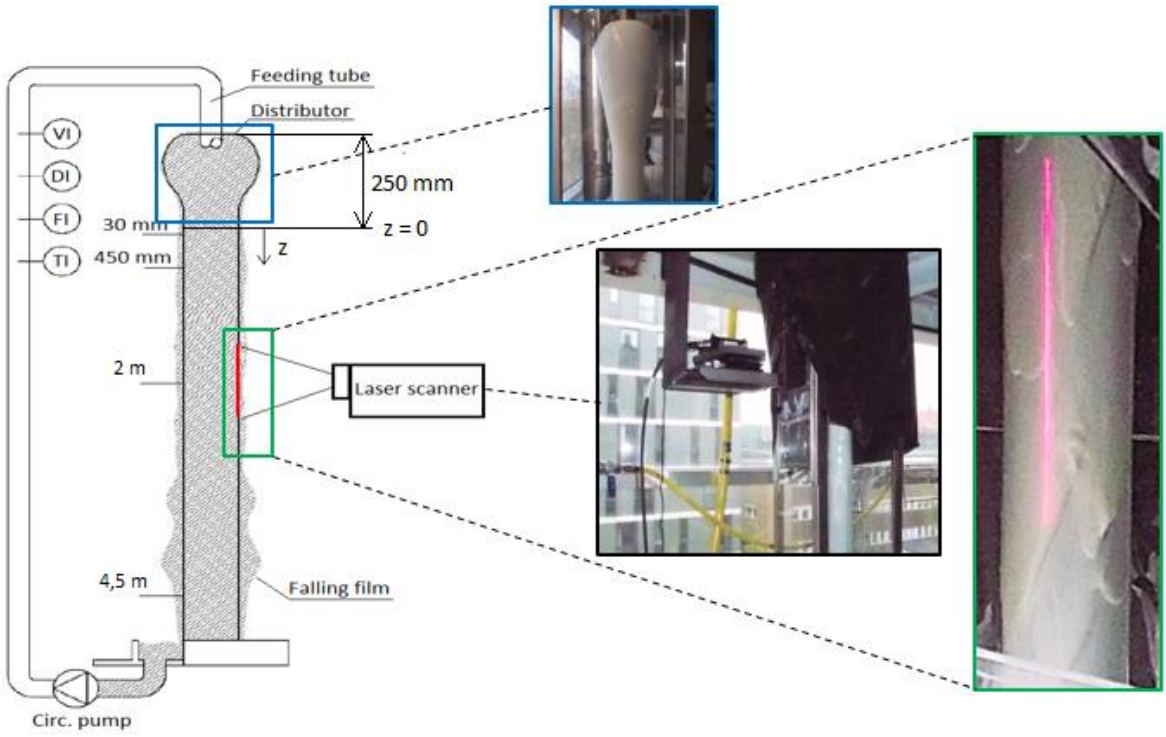

Figure 5.1: Schematic sketch of the test facility: DI=Density meter, FI=Flow meter, TI=Temperature meter, VI=Viscometer (Akesjö et al., 2015).

Table 5.1: Quantity and accuracy of the measurement instruments (Akesjö et al., 2015).

Quantity	Instrument	Accuracy
Temperature	PT-100, ABB H210, H600	± 0.2 K
Mass flow rate and density	Endress + Hauser PROline promass 80 H	± 0.20 % of range
Viscosity	Marimex, Viscoscope Sensor VA-300L	± 1.0 % of value

5.2 Laser measurement device

For the visualization of the falling liquid film an optical triangulation scanner (light intersection method) of the model scanCONTROL 2950-100 from Micro-Epsilon (Micro-Epsilon. Laser-Scanner Manual, n.d.). It uses a 20mW power source to project a laser line on the target surface via a linear optical system. The laser line is reflected as diffuse light and is replicated on a sensor array by a high accuracy sensitive optical system. It measures the reflected angle in 1280 points along the projected red line, see *Figure 5.1*. With the angle the distance to the surface can be determined. The measuring range x, depending on the distance, is determined by an inbuilt camera. The scanner samples at a frequency of 500 Hz and a resolution of $\pm 1.2 \cdot 10^{-5}$ m. The nonlinearity, i.e. deviation from true value is ± 0.16 %, based on the full scale output (Akesjö et al., 2015)Akesjö et al., 2015*;* Micro-Epsilon. Laser-Scanner Manual, n.d.).

In the test facility the scanner is used to continuously measure the distance $z_i(x)$ to the falling film surface along a vertical path, visualized as red line, see *Figure 5.1*. The film-thickness at each point along the line (1280) can be calculated by $h(x) = z_r(x) - z_i(x)$, where $z_r(x)$ represents the reference distance measured between the scanner and a surface without falling film flow (Akesjö et al., 2015 Micro-Epsilon. Laser-Scanner Manual, n.d.).

One crucial limitations for the laser device is the liquid as it has to be optical reflecting. Therefore a dairy product is used. It has a white colour and thus good optical reflecting properties for the wave-length of the laser-light. Further the dairy product offers the advantage to easily adjust the viscosity of the liquid by changing the solid content. By this the influence of different fluid properties respectively the influence of Ka can be investigated. Within this work, the flow pattern for solid contents of 10 % and 30 % are investigated.

Calibration of the laser

As different solid contents of the dairy product may influence the optical reflecting properties, a calibration of the laser measurement device has been performed with the help of a micrometer. The setup is shown in *Figure 5.2*.

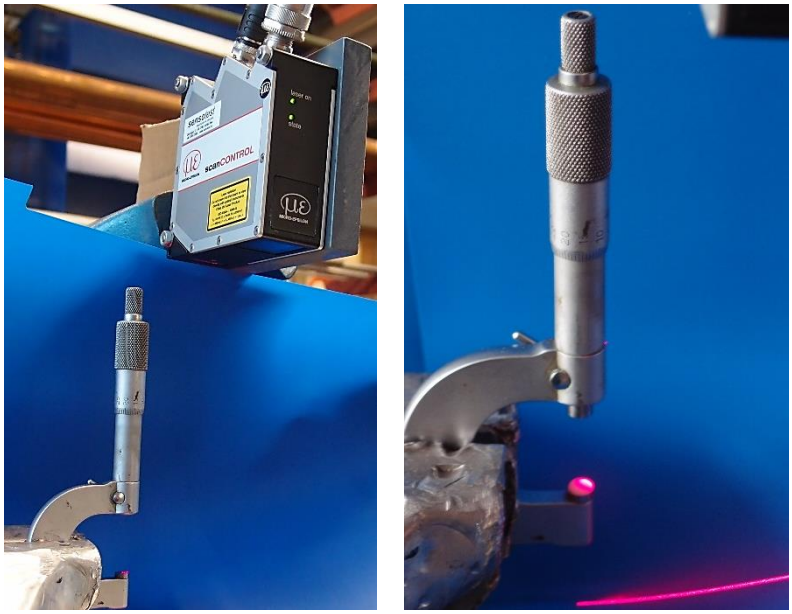

Figure 5.2: Setup for the calibration of the laser measurement device including a micrometer and the laser device (left picture). The right picture shows the measured droplet of a dairy product.

First the reference distance to the surface of the micrometer without droplet is measured (*Figure 5.2* left). Then a droplet of a dairy product is placed on the micrometer (*Figure 5.2* right). The maximum thickness of the droplet is first determined with the laser device and secondly with the calibration instrument (micrometer). The result of the calibration showed, that the laser device can measure the film thickness with an accuracy of 0,1 mm down to a minimum solid content of approximately 4 %.

Validation of the laser measurement results

For the validation of the laser measurement results, repetitions of experiments have been done and the results compared with each other (Appendix 11.9). Further the results of the total mean film thickness $\bar{h}$ have been compared with film thickness correlations of previous publications (Chapter 7.1).

6 Method

In this chapter first the method applied for data pre-processing is shown. Therefore the "raw" data, extracted from the laser device are pre-treated before they are evaluated. This is followed by data processing. Presented are the methods which are applied to evaluate the parameter of interest (chapter 4) to describe the liquid flow pattern.

6.1 Data cleaning/Pre-processing

Raw datasets can be noisy due to measurement errors, the environment (light, reflection, vibration) as well as by the occurrence of outliers (falling droplets). These influences have a negative impact on the evaluation as they lead to inaccuracy of the results. Therefore data pre-processing is needed to evaluate the data gained from the laser measurement device. The target of data pre-processing is to gain a more compact (reduced amount of data) and clean dataset with a higher accuracy.

The raw film thickness data extracted from the laser device are returned in an array. The number of columns is fixed by the number of measurement points within the laser measurement range, thus 1280 points. The length of the rows depends on the time of measurement. As the laser measures with a frequency of 500 Hz, each second results in a total amount of 640.000 instantaneous film thickness data. The method of data pre-processing applied in this thesis is shown as an example for the experiment in following table, where z is the distance from liquid inception and $\dot{V}$ the volume flow:

Table 6.1: Dataset used for showing the method for data pre-processing

Exp. Nr.	t [ms]	z [mm]	$\dot{V}$ [l/h]	Ka	Re	$\bar{h}$ [mm]
4	11.090	450	200	$5{,}6 \cdot 10^9$	171	0,69

The *first cleaning step* is to exclude columns of the dataset containing NaN (Not-a-Number) values, related to measurement errors.

Second cleaning step is to exclude outliers due to the standard deviation Std_m of the mean film thickness. Therefore the time averaged mean $\bar{h}_i$ for each position i, the total mean film thickness $\bar{h}$, averaged over time and position as well as the standard deviation Std_i of $\bar{h}_i$ is calculated. The mean over all Std_i results in Std_m. These calculated values are shown in *Figure 6.1*. All columns of the film thickness data, where the mean of the point exceeds the standard deviation Std_m are excluded and thus deleted. Std_m is used as it represents a good value to exclude noise. Noise has been identified by comparison of film thickness traces synchronized with movies of the high speed camera. For a range of measurement conducted, noise strongly occurs around 460 mm, 500 mm and 550 mm. In the middle of the measurement range the laser is not able to measure good values because of reflexions. The columns around this position contain the most negative values. With this cleaning step a reduction to 838 columns and thus a more compact array of the film thickness is achieved. Thus by applying this method the amount of data of the raw dataset are reduced (reduction in computing time) to a cleaner dataset with a higher accuracy.

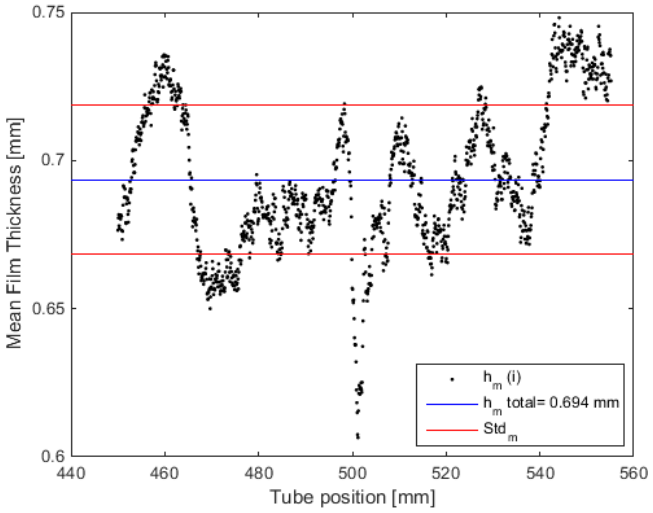

Figure 6.1: Mean film thickness over tube position $h_m(i)$ (black), total mean of film thickness $h_m total$ (green) and standard deviation of mean film thickness Std_m (red).

The accuracy due to outliers still has to be improved. The resulting film thickness data still contain negative values corresponding to measurement errors which have to be removed. To make this *third cleaning step* not as complex, rows where negative values are existing are deleted. This has a big influence on $\bar{h}_i$, especially in the middle of the measurement range, as they have damped outliers. In *Figure 6.2* it can be seen that the values gain "much" higher values again. Therefore a final *fourth cleaning step*, following the same procedure as in step two exclude these outliers, due to Std_m. The result after this cleaning step are the values between the two red lines (Std_m). These values are defined as a "clean dataset", which is more compact and has an accuracy high enough for data processing and evaluation.

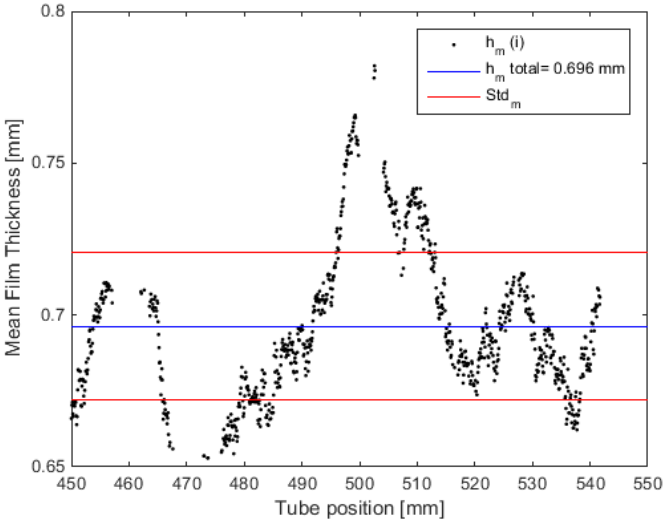

Figure 6.2: Mean film thickness $h_m(i)$ (black), total mean of film thickness $h_m total$ (blue) and standard deviation of mean film thickness Std_m (red) while cleaning.

6.2 Instantaneous film thickness data

In the following, the method for the evaluation of instantaneous film thickness data are shown, namely the total mean film thickness $\bar{h}$, substrate thickness h_s, wave amplitude A and mean wave velocity u, Film thickness distribution and probability density function PDF.

6.2.1 Mean film thickness

The total mean film thickness $\bar{h}$ and its determination has already been investigated in detail in chapter 6.1 ("Data cleaning"). The total mean film thickness $\bar{h}$ is the average over measurement time and positions within the laser measurement range. This value give a first statement about the development of the flow and the accuracy of the measurement. Downstream, a thinning in the film is expected as the velocity of the liquid increases due to gravity. The results of $\bar{h}$ are compared with film thickness correlations of other researchers and thus give a good comparison for the validation of the results.

6.2.2 Substrate thickness (Probability Density Function PDF)

The film substrate thickness h_s is determined by application of the probability density function PDF. Therefore first a film thickness distribution is evaluated. It represents the density/frequency of all instantaneous film thickness values. The substrate thickness h_s is defined as the film thickness with the highest frequency/density. The PDF builds the fit to the film thickness distribution, see *Figure 6.3*.

The distribution is asymmetric, with dense thickness data in the low thickness range compared to a sparser distribution in the high thickness range. The peak (0,94 mm, green line) corresponds to the most frequent thickness and is referred to as substrate thickness h_s. The PDF is skewed to the right to higher film thickness values, contributed to the occurrence of waves. The PDF in comparison to the film thickness distribution gives the possibility to compare different experiments within on graph more easily. Doing this a first estimate of the influence of different flow properties Ka, Re) on the flow pattern can be made.

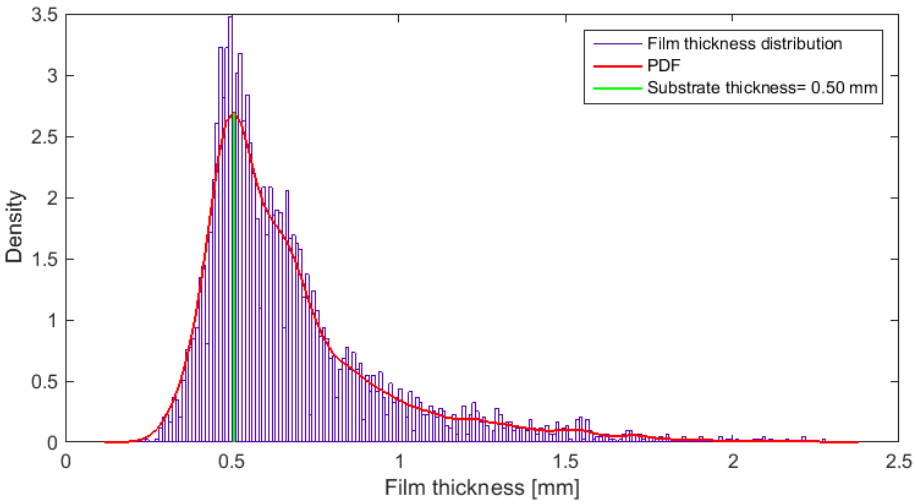

Figure 6.3: Film thickness distribution, PDF and substrate film thickness

Mascarenhas and Mudawar show by usage of the probability density, that with increasing Re the film thickness shifts to higher values, seen by a flattening in the probability density curve with a higher range of film thickness values and a lower peak density. The flattening of the curve, respectively the width of distribution indicates an increase in the wave amplitudes (Mascarenhas and Mudawar, 2014). Al-Sibai observed a flattening and widening of the curve with decreasing Ka.

6.2.3 Wave amplitude

As a global definition of a wave especially it´s classification doesn´t exist so far, a new method, which hasn´t been found in the literature is presented here. The experiment used to exemplify this is the same as shown in *Table 6.1*. A film trace over around 1200 ms at one point of laser measurement range is drawn in *Figure 6.4*. Displayed are the film thickness trace (black solid line), its corresponding maxima and minima, the mean film thickness h_m (blue dashed line), the substrate film thickness h_s (green dashed line), the standard deviation of the mean film thickness Std_m and two times the standard deviation $2xStd_m$.

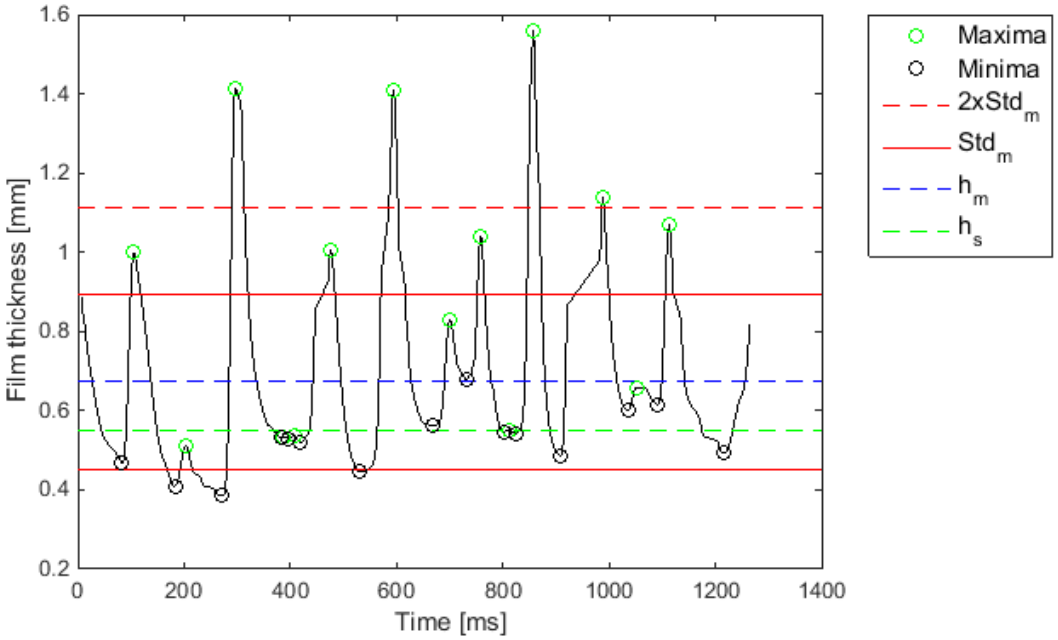

Figure 6.4: Example for a film thickness trace including local maxima and minima, standard deviation Std_m,mean film thickness h_m and substrate film thickness h_s.

At first the amplitudes of all local film thickness fluctuations are calculated according to Chu and Dukler (4.3) using the maxima and the average minimum in front and back of the wave through. These amplitudes are then classified into different wave types/sizes due to the location of their local maxima (Range). These classifications can be seen in following *Table 6.2*:

Table 6.2: First classification of wave due to it´s maxima

Type	Range
No Wave	$Maxima < h_s$
Substrate Wave	$h_s < Maxima < \bar{h}$
Small Wave	$\bar{h} < Maxima < \bar{h} + Std_h$
Big Wave	$\bar{h} + Std_h < Maxima < \bar{h} + 2xStd_h$
Large Wave	$\bar{h} + 2xStd_h < Maxima < \bar{h} + 5xStd_h$
Outliers	$Maxima > \bar{h} + 5xStd_h$

The table shows six different ranges for the classification of the waves due to the location of it´s maxima. Chu and Dukler defined the smallest wave as the substrate wave which a maxima and minima below $\bar{h}$. This definition for a substrate wave has been modified here with a maxima, which has to be also higher than the mean substrate film thickness h_s. This follows that small amplifications, below h_s, do not correspond as a wave.

The classifications "ranges" of the "small", "big", and "large" wave maxima have been chosen due to visual observations of different film thickness traces as for example seen in *Figure 6.4*. "Outliers" are defined by a maxima exceeding five times the standard deviation of $\bar{h}$. Doing this outliers as falling droplets are excluded.

For comparison of different flow properties, only the small, big and large waves are taken into account, thus only waves with a local maxima higher than $\bar{h}$. These "bigger" waves have the most influence on the substrate (thinning) as well as represent the transitions regimes by an increase or decrease in the wave crest. However to also include smaller fluctuations, the standard deviation Std for different flow properties is used.

The *first classification* of the waves has been done due to the location of the maxima but does not take into account the location of the local minima. If the local minima are very close to the maxima the resulting A is as small as a substrate wave but still counts to the "bigger waves". Therefore a second classification due to wave amplitudes is defined to exclude the influence of the small fluctuations on the "bigger waves". This can be seen in *Table 6.3*. The reason and determination of these *second classification* can be seen in Appendix 11.1. Where three different ranges are investigated, whereas the here presented range gives the most satisfying results.

Table 6.3: Second classification due to wave amplitudes: Three different ranges are investigated

Wave	SMALL	BIG	LARGE
Range	$A > \frac{1}{2} * Std_h$	$A > Std_h$	$A > 1{,}5 * Std_h$

Out of these classifications the mean wave amplitude of the large waves $\bar{A}_{Large}$ (6. 1) and the total mean wave amplitude $\bar{A}$ are determined. $\bar{A}$ is calculated as the mean of the small, big and large wave amplitudes (6. 2). The wave amplitudes have been investigated at 30 points along the laser measurement range to get a higher range of investigated points and therefore a more accurate result of the mean as more data are considered.

$$\bar{A}_{Large} = \frac{1}{n_{Large}} \sum_{i=1}^{n_{Large}} A_{Large}(i) \qquad (6.1)$$

$$\bar{A} = \frac{\sum_{i=1}^{n_{Large}} A_{Large}(i) + \sum_{i=1}^{n_{Big}} A_{Big}(i) + \sum_{i=1}^{n_{Small}} A_{Small}(i)}{n_{Large} + n_{Big} + n_{Small}} \qquad (6.2)$$

It is expected that $\bar{A}_{Large}$ shows a change of the flow pattern respectively flow regimes more pronounced as compared to $\bar{A}$ and Std .

6.2.4 Wave velocity

The wave velocity is determined using signal cross-correlation between two film thickness signals at two different positions. The cross-correlation detect signal similarities and makes it possible to detect the lag, thus the time difference between the maxima within the compared signals. This is pictured in *Figure 6.5*. The wave velocity is then calculated as seen in (6.3):

$$u_i = \frac{z_2 - z_1}{\Delta t} \qquad (6.3)$$

To determine more velocities within one film thickness trace, the time range of the film thickness trace is staggered and the cross-correlation is applied within each stage. Furthermore, the cross-correlation is applied between different positions within the laser measurement range to further increase the accuracy of this method and detect outliers. Finally a mean wave velocity u is determined, which is used for comparison between different flow properties.

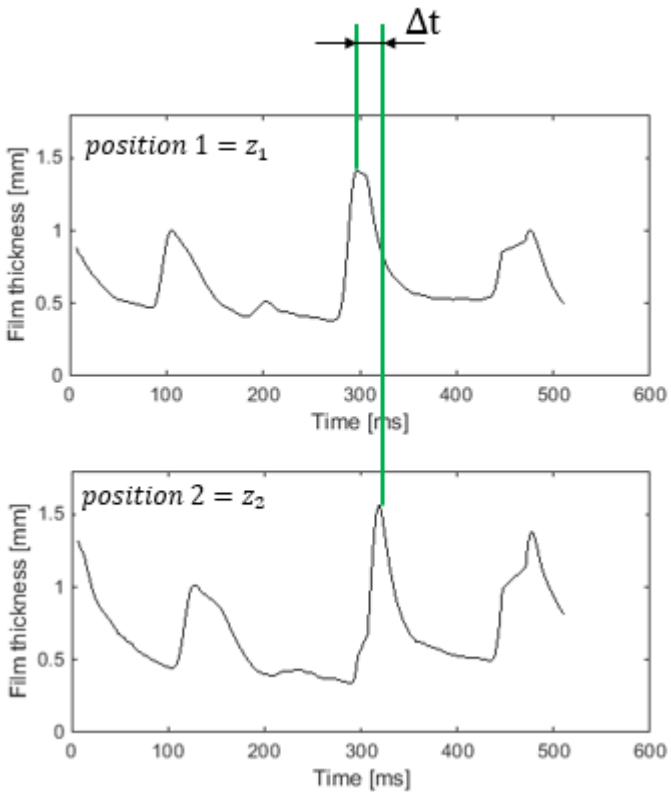

Figure 6.5: Determination of the wave velocity by signal-cross-correlation between two signals. Δt represents the time lag between the two maxima.

6.2.5 Wave frequency

The determination of the frequency is done by using the Fourier-Transformation, in which the instantaneous film thickness measurement is broken down into the sum of individual sin waves and converted from the time domain to the frequency domain. These method has already been applied by Patnaik and Perez-Blanco, 1996 as well as Al-Sibai, 2004.

7 Results

The film thickness parameter are investigated at different positions (30 mm, 450 mm, 2 m and 4,5 m) over a range of Re and two different $\overline{Ka}$. $\overline{Ka}$ represents the mean Ka over all experiments either for the low or high solid content. The experiments for the high solid content (30 %) result in a dynamic viscosity $\mu = 6{,}68 \pm 0{,}58$ mPas. The experiments for the low solid content (10 %) result in $\mu = 1{,}72 \pm 0{,}18$ mPas. These viscosity result in $\overline{Ka}$ of $6{,}91 \cdot 10^6$ and $1{,}56 \cdot 10^9$ for the high and low solid content respectively.

For better characterization of the different flow regimes, the Re_{crit} from different authors (*Table 2.1*) have been calculated according to these $\overline{Ka}$. The results are shown in Appendix 11.1.

7.1 Mean film thickness

In *Figure 7.1* and *Figure 7.2* the mean film thickness is presented against Re for the high and low $\overline{Ka}$ respectively. Included are the correlations of $\bar{h}$ by Nusselt for laminar flow and Lukach for wavy-laminar flow.

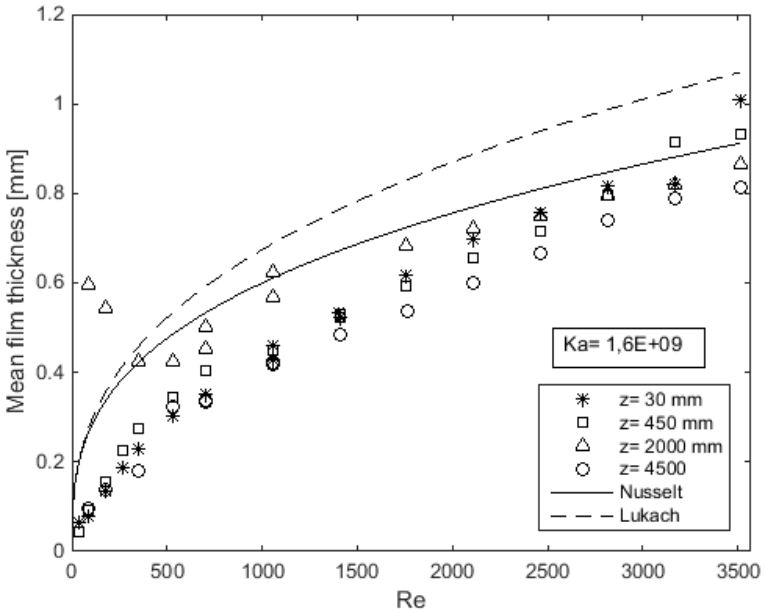

Figure 7.1: Mean film thickness against Re at different positions for $\overline{Ka} = 1{,}6 \cdot 10^9$. Solid line and dashed line represent the estimated film thickness according to Nusselt for laminar flow and Lukach for wavy-laminar flow respectively.

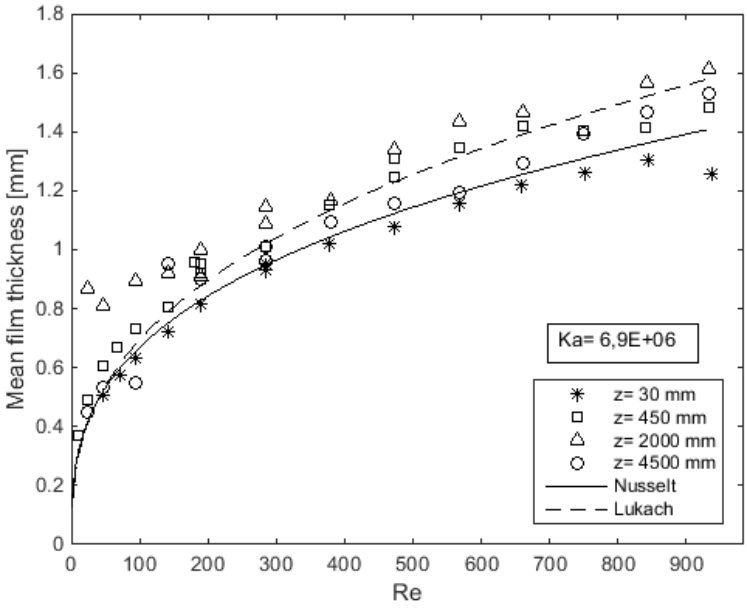

Figure 7.2: Mean film thickness against Re at different positions for $\overline{Ka} = 6{,}9 \cdot 10^6$. *Solid line and dashed line represent the estimated film thickness according to Nusselt for laminar flow and Lukach for wavy-laminar flow respectively.*

For the low $\overline{Ka}$ at 30 mm the Nusselt correlation for laminar flow represent a good fit. At a Re higher than 900, overshooting occurred at the distributor, resulting in a decrease of $\bar{h}$ (outlier). At 450 mm the correlation of Lukach for wavy-laminar flow represents a good fit. For the high $\overline{Ka}$ both correlations overestimate $\bar{h}$. The reason for this behaviour is not clear. It could be an influence of the different solid contents of the liquid as well as that the correlations have been determined for a falling film on a flat plat, different to the experimental setup used here. However the measurements, follow the trend of Lukach's correlation with a difference around 0,2 mm.

For the *longitudinal development* the points of $\bar{h}$ at a certain Re are compared vertically.

It is expected that $\bar{h}$ is thinned in the flow direction thus the value get lower downstream. The velocity of the falling film increases downstream, accelerated by gravity. Due to mass conservation this forces a thinning of the film. For the positions at 2 m and 4,5 m the expected film thickness development is valid, decreasing downstream for both $\overline{Ka}$. At the positions of 30 mm and 450 mm the results are different.

For the high $\overline{Ka}$, $\bar{h}$ is thicker at 450 mm than at 30 mm up to a $Re = 703$, then changes with a thinner $\bar{h}$ at 450 mm. For the low $\overline{Ka}$, $\bar{h}$ is always thicker at 450 mm over the total range of Re. This behaviour is different than expected concerning the theory of film thinning by increase in film velocity downstream.

This effect may be contributed to the formation of waves, starting to form shortly after the measurement position at 30 mm from fluid inception. The waves grow by picking up fluid at the wave through and thus causes a thinning of the film. At the position of 30 mm therefore this thinner film may be measured. This effect is pictured in following *Figure 7.3*.

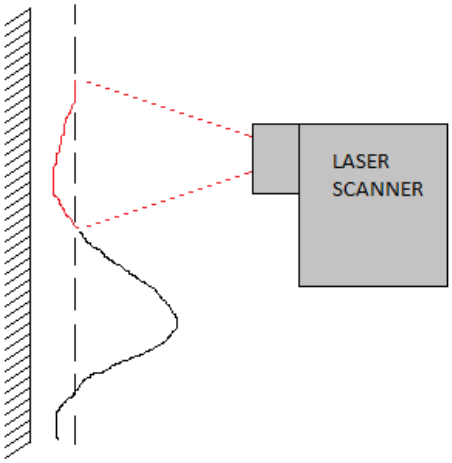

Figure 7.3: Effect of substrate thinning on laser measurement. Laser shows a thinner result for the mean film thickness as only the film at the wave through is measured, not the wave crest.

Further downstream of the measurement position at 30 mm seen in *Figure 7.3*, at a position of 450 mm these waves can already be measured and thus show a higher $\bar{h}$. These effect has already been mentioned by Salazar and Marschall, 1978 and Drosos et al., 2004.

At the position $z = 2$ m and a volume flow below $\dot{V}$ around 200 l/h corresponding to approximately $Re = 200$ for low $\overline{Ka}$ and $Re = 700$ for high $\overline{Ka}$, $\bar{h}$ behaves the opposite in comparison to the other positions. It increases with decreasing $\dot{V}$. This effect is especially notable for a high $\overline{Ka}$.

During the experiments it has been observed that the pipe is slightly bended in the middle, almost not visible by eye. With lower $\dot{V}$ corresponding to a lower film velocity, the liquid has "more time" and is driven by gravity to the position/side of the pipe where the angle between a horizontal and the pipe surface is the smallest. This fact leads to an uneven distribution of the liquid film. Wetting problems occurred and got especially high at $\dot{V} < 100\ l/h$ where dry outs have been observed. The effect is lower for the low $\overline{Ka}$ as the development of roll waves start at a shorter distance of fluid inception (described in following chapters). The main forces acting on roll waves are inertia and gravity. When roll waves appear these forces overweight compared to the driving force of the liquid following the bended pipe. The influence of the bended pipe decreases.

The effect of the bended pipe makes it difficult to give an comparable investigation of the longitudinal flow development downstream of 450 mm for $\dot{V} < 200\ l/h$. The results at 30 mm and 450 mm are not influenced by this effect, as a different setup with a shorter pipe was used.

7.2 Standard deviation Std

The standard deviation Std is a measure of dispersion and show how the film thickness fluctuates about their mean. This values are shown for all distances and both $\overline{Ka}$ in *Figure 7.4*. On the left side of the Figure (Black) the results of Std are presented for $\overline{Ka} = 6{,}9 \cdot 10^6$ whereas on the right side Std for $\overline{Ka} = 1{,}6 \cdot 10^9$ are presented.

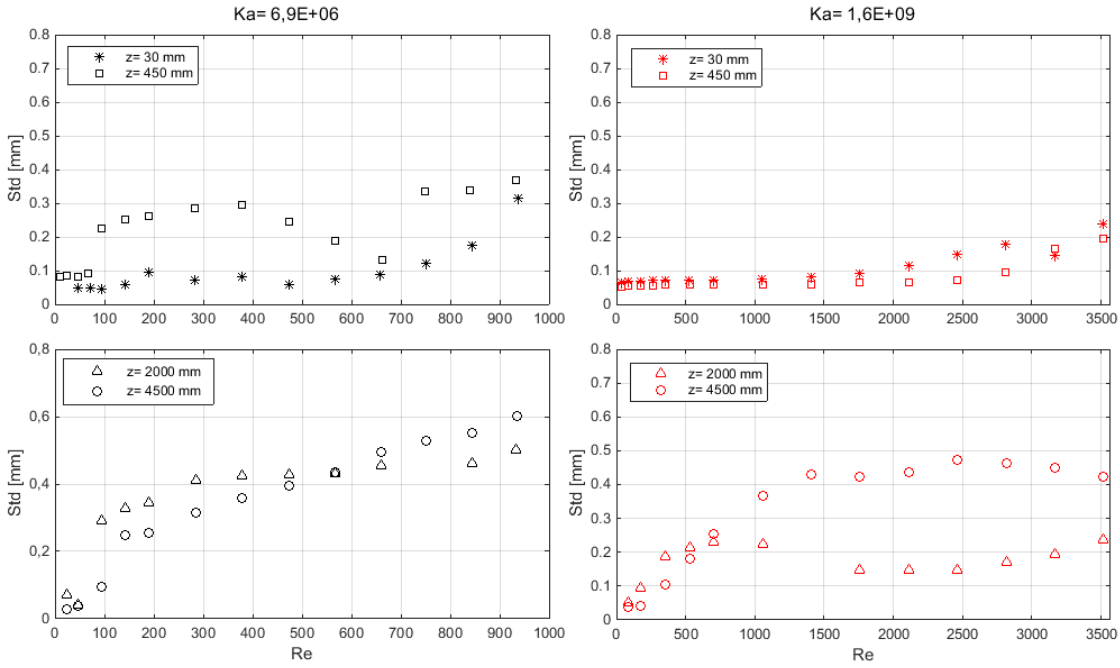

Figure 7.4: Standard deviation Std of $\bar{h}$ at 30 mm, 450 mm, 2000 mm and 4500 mm against Re for $\overline{Ka} = 6{,}9 \cdot 10^6$ (black, left) and $\overline{Ka} = 1{,}6 \cdot 10^9$ (red, right)

<u>Std for high $\overline{Ka}$</u> (*Figure 7.4* red right)

At 30 mm, Std remain almost constant between 0,05 – 0,08 mm up to $Re \cong 1500$ then increases linearly. The Std at 450 mm stays approximately constant between 0,05 – 0,08 mm up to $Re \cong 2500$ then increases as well. The region up to $Re \cong 1500$ points to a smooth film with small waves on the substrate. Roll waves thus start to develop downstream of 450 mm from liquid inception.

The point where the difference between Std differ increasingly ($Re \cong 1500$) is approximately the same as seen in *Figure 7.1* where $\bar{h}$ at 30 mm gets thicker than at 450 mm. This may be a point presenting a Re at which the development of the waves start earlier than the measuring position at 30 mm from inlet.

The fact that Std is higher at 30 mm than 450 mm points to small waves (capillary waves) with higher amplitudes upstream which decrease again to 450 mm. This may be contributed to surface tension damping the wave amplification. The difference however is really small so that it could also be related to an inaccuracy of the measurement.

The wave amplitude increases further downstream seen by comparing the Std at 2 m and 4,5 m. At both positions a peak in the Std with following decrease can be observed. The point where Std decreases points to a decay of the wave crest by strengthened wave collision/interaction.

However at $z = 2\,m$ it is difficult to make a statement if the peak is related to a *decay* in the *wave crest* or by the *influence of the bended pipe*. For lower Re the liquid film follows the bended pipe thus results in a falsified value of h (see 7.1) and thus falsified wave development corresponding to the local Re. At this position the peak may represents a point where the inertia forces of the liquid film and waves start overweighting. The influence of the bended pipe decreases. At a $Re > 1500$ (volume flow > 400 l/h) the development is more comprehensible.

At 4,5 m for high Ka the maximum in the Std is around $Re \cong 2500$. According to Patnaik and Perez-Blanco, 1996 this Re is placed in the inertia-wavy-turbulent flow regime ($1000 \leq Re \leq 4000$) where increasing wave collision/interaction leads to decreasing wave amplitude. According to Al-Sibai, 2004, who defined the flow regimes dependent on Ka (*Table 2.1*) the point of transition to full turbulent flow results in a Re between 672-2735 for a $Ka = 1{,}6 \cdot 10^9$. Thus the decrease in Std may be related to a *transition to fully turbulent flow.*

<u>Std for low Ka</u> (*Figure 7.4* black left)

The effect of the bended pipe seems to be less for a lower Ka at 2 m as a significant peak with following decrease not exist. The wave formation at a lower Ka starts earlier at around 450 mm and a $Re \cong 100$ with follows inertia forces of the waves overweighing the influence of the bended pipe. The significant jump in Std at this position shows the occurrence of larger waves. Thus it is expected that there might be a *transition from the capillary-wavy-laminar to the inertial-wavy-laminar flow regime.*

Patnaik and Perez-Blanco, 1996a reported that the capillary-waves (sinusoidal waves) are existing between $Re \cong 20 - 200$ whereas Al-Sibai defined the limit of the capillary waves dependent on Ka (*Table 2.1*), resulting in a $Re \cong 19$ for $Ka = 6{,}9 \cdot 10^6$. Ishigai et al., 1972 reported the transition to wavy-laminar flow regime also dependent on Ka resulting in a $Re = 43$. It has to be mentioned that the experiments from Al-Sibai have been made on a liquid film falling down a flat plate. In this case the transition at 450 mm takes place between a local $Re = 66 - 95$. This is investigated in more detail by the application of the probability density function (PDF) in the next chapter.

Between $Re = 400 - 800$ (450 mm), the Std shows a peak with following decrease and a rapid increase (jump) again from around 0,1 mm to 0,4 mm ($Re \cong 750$). The peak with following decreases shows strengthened wave interaction/collision leading to decreasing wave amplitudes. This is getting stronger with increasing volume flow. The point where the Std jumps again may represents a Re where the point of wave collision may move downstream of 450 mm. After the wave collision waves start again to form. The higher the film thickness the bigger the wave amplitude can be. However as the point of wave collision moves downstream the distance between this point and the position at 2 m gets less and thus the length for the wave development does. This follows that an increase in wave amplitude is limited and Std at 2 m only increases slightly.

At 4,5 m, Std shows a linearly increasing behaviour. A transition regime or wave collision is therefore not expected. The linear increase is the same for both Ka between a range of $Re \cong 150 - 1000$.

7.3 Probability density function PDF

In the following the results of the probability density function for different experiments are investigated. The PDF is investigated at different positions for different Re and Ka.

Investigation of $Re < 200$ for $Ka = 6,9 \cdot 10^6$

To investigate the expected transition from capillary-wavy laminar into inertia-wavy laminar regime, the PDF at a position of 450 mm and a $Ka = 6{,}9 \cdot 10^6$ for the lower Re range $Re = 20 - 200$ is shown in *Figure 7.5*.

Between $Re = 47 - 66$ the PDF has a sharp peak with a dense film thickness distribution symmetrical around the peak. A sharp peak with dense film thickness distribution about the mean points to a purely laminar or capillary-wavy-laminar flow. According to investigations of different researchers, a purely laminar flow exist only up to a $Re = 20$ (see *Table 2.1* and *Table 11.3*). Therefore the PDF at these two Re correspond to a capillary-wavy-laminar flow with increasing amplitude by an increase in Re. In *Figure 7.5* this can be seen by a decrease in the density of the peak as well an increase in width of distribution.

With a further increase to $Re = 95$ the distribution changes significantly, gets more flat with the peak moving to the left. The curve shows a high skewness of the distribution implying the existence of "larger waves". The substrate thickness h_s decreases from 0,67 mm to 0,54 mm although the volume flow increases. This is related to the existence of waves. Especially roll waves are known to travel downstream over the substrate with an increase in speed and wave amplitude by picking up fluid from the film substrate, thus thinning the substrate. This phenomenon can be seen here.

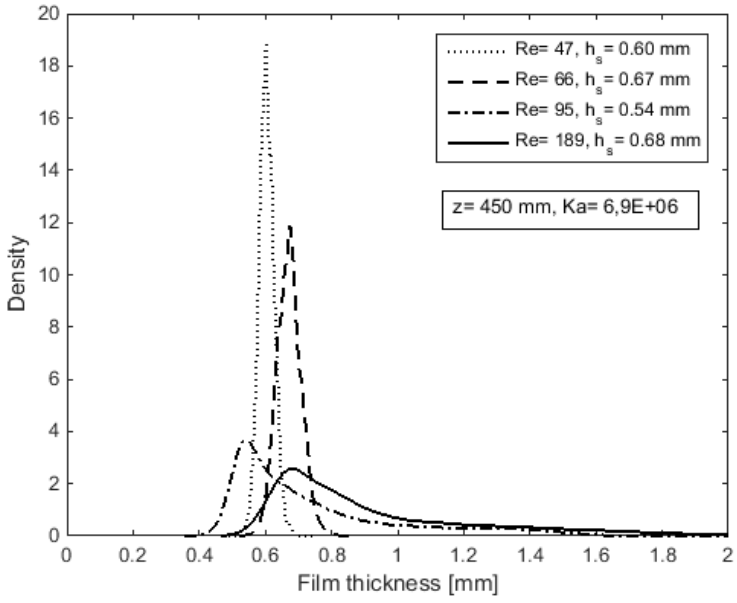

Figure 7.5: PDF at 450 mm with $Ka \cong 6{,}9 \cdot 10^6$ *and* $Re = 47 - 189$ *(h_s=substrate thickness).*

To picture this transition between $Re = 66 - 95$ more intensively the film thickness traces for $Re = 66$ and $Re = 95$ over a measuring range of 2000 ms are shown in *Figure 7.6*. For $Re = 66$ the film thickness trace reminds on a sinusoidal function. The waves fluctuate by approximately $\pm 0{,}05mm$ (symmetrically) around the value of h_s (green line). At $Re = 95$ amplitudes increases significantly, roll waves occur, and the substrate gets thinner. The film thickness trace represents one point within the laser measurement but shows similar traces at other points.

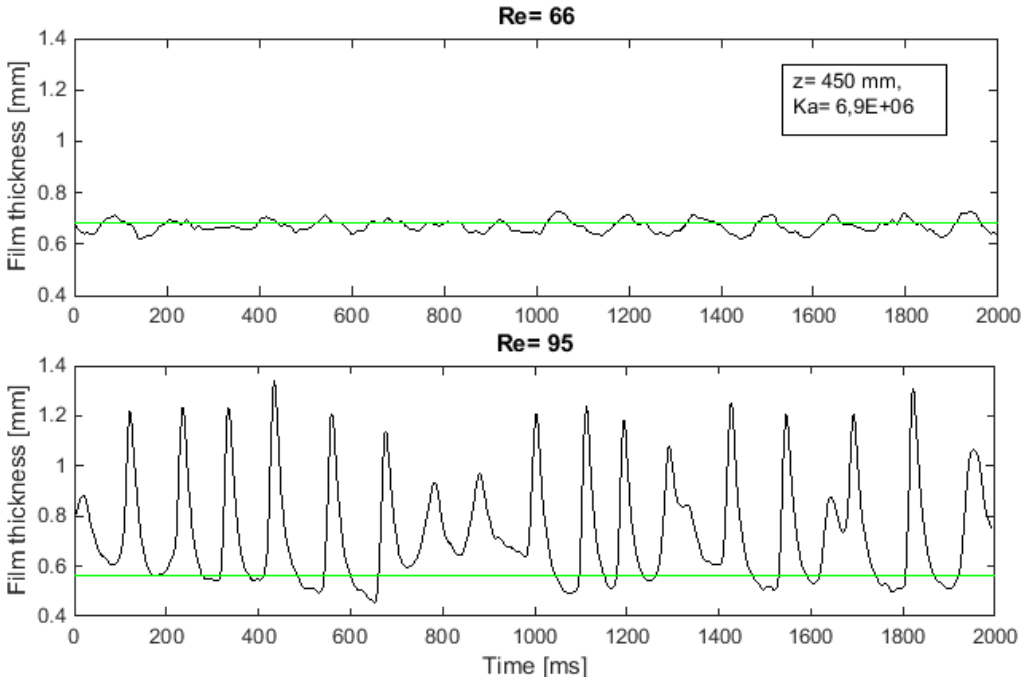

Figure 7.6: Film thickness trace at $450\,mm$, $Ka \cong 6{,}9 \cdot 10^6$ *for* $Re = 66$ *(top) and* $Re = 95$ *(bottom). Green line represents* h_s.

In the Appendix 11.1 all film thickness traces due to *Figure 7.5* are presented and more information about the maximum and minimum fluctuations are given. Further the transition is shown by comparison of $\bar{h}$ and h_s, showing a first difference after the transition.

The conditions upstream of 450 mm, at a position 30 mm can be seen in *Figure 7.7*. Compared to 450 mm the flow regime at $Re = 95$ still shows the distribution of a capillary-wavy laminar flow with a sharp peak. At $Re = 189$ the density of the peak decrease significantly and a complete symmetry is not given anymore. Capillary-wavy laminar flow still overweight but the PDF shows a slight skewness to the right. The point of wave formation moved upstream to 30 mm.

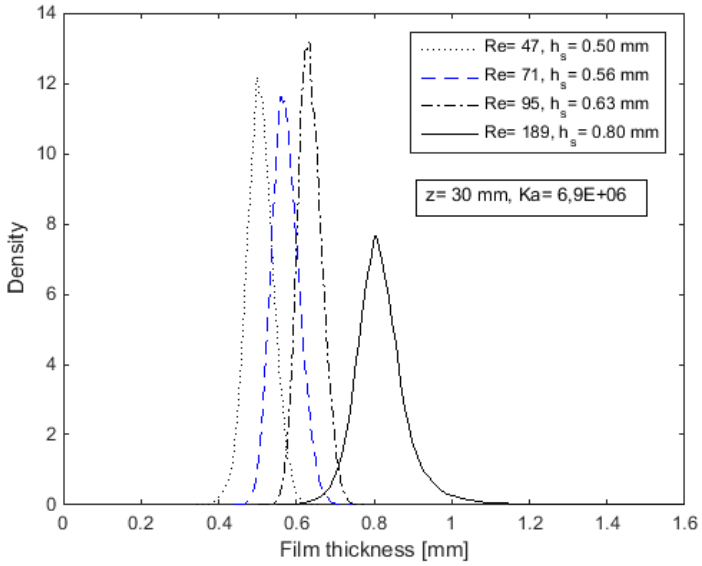

Figure 7.7: PDF at 30 mm with $Ka \cong 6{,}9 \cdot 10^6$ *and* Re *=47-189 (*h_s*=substrate thickness).*

In the following the longitudinal flow development is investigated by application of the PDF at both Ka and range of Re, at which the influence of the pipe is less respectively can be neglected.

PDF for low Ka (*Figure 7.8*)

In *Figure 7.8* the longitudinal development for different volume flows (Re) for an average $Ka = 6{,}9 \cdot 10^6$ is presented.

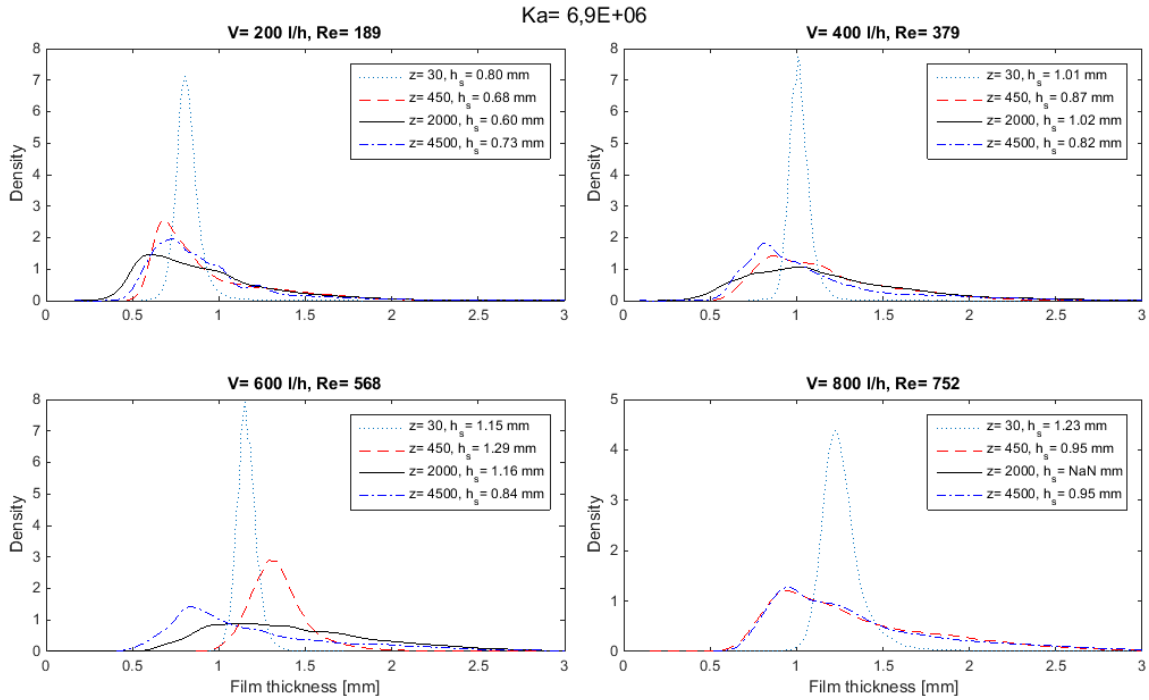

Figure 7.8: PDF at all positions for, $Ka \cong 6{,}9 \cdot 10^6$ *for different Re*

At 30 mm and 200 l/h as shown before the point of transition into the inertia-wavy-laminar flow starts around 30 mm. Capillary-wavy-laminar flow overweight but waves with higher amplitudes occur. At 450 mm the inertia-wavy-laminar flow regime is present, roll-waves occur thinning the substrate (PDF shows high skewness, peak moves to the left).

Downstream at 2 m, wave amplitude increase further and h_s decreases. At 4,5 m h_s increases again contributed to decrease in wave amplitude. Further the peak of the PDF gets less pronounced. This behaviour is typical for the inertia-wavy-turbulent flow regime where strengthened wave collision/interaction lead to a decrease in wave amplitude and increase in h_s. Ishigai et al., 1972 presented a value of $Re \cong 300$ for the transition into the inertia-wavy-turbulent flow regime. However this value may not be valid as a global critical Re. His investigations were made on a 2 m pipe and he mention that this length may not be enough to give a true value for Re_{crit} (Ishigai et al., 1972). In this case the transition to inertia-wavy-turbulent flow regime may take place already at $Re \cong 189$.

At 400 l/h and 600 l/h the effect of decay in wave crest moves upstream to 450 mm and reaches it maximum with a high decay in wave crest at 600 l/h at a position of 450 mm. The PDF developed to a curve similar to the form of a Gaussian normal distribution. The substrate thickness $h_s = 1{,}25$ mm reaches almost $\bar{h} = 1{,}34$ mm. At this position and $\dot{V}$ the flow has turbulent flow pattern. However further downstream waves develop again transform into larger roll waves at 4,5 m. The substrate is pronounced and is between 0,82 – 0,84 mm at 400 l/h and 600 l/h respectively.

At a volume flow of 800 l/h ($Re = 752$) the PDF is approximately the same at 450 mm and 4,5 m pointing to a fully developed interia-wavy-turbulent flow at these flow properties.

PDF for high $\overline{Ka}$ (*Figure 7.9*)

The longitudinal flow development for the higher $\overline{Ka} \cong 6{,}9 \cdot 10^6$ is shown in **Error! Reference source not found.**. Due to the higher influence of the bended pipe at this Ka for lower $\dot{V}$ the PDF shown starting from a volume flow at 400 l/h. The PDF for low $\dot{V}$ at the shorter distances of 30 mm and 450 mm are shown separately seen in Appendix 11.6.

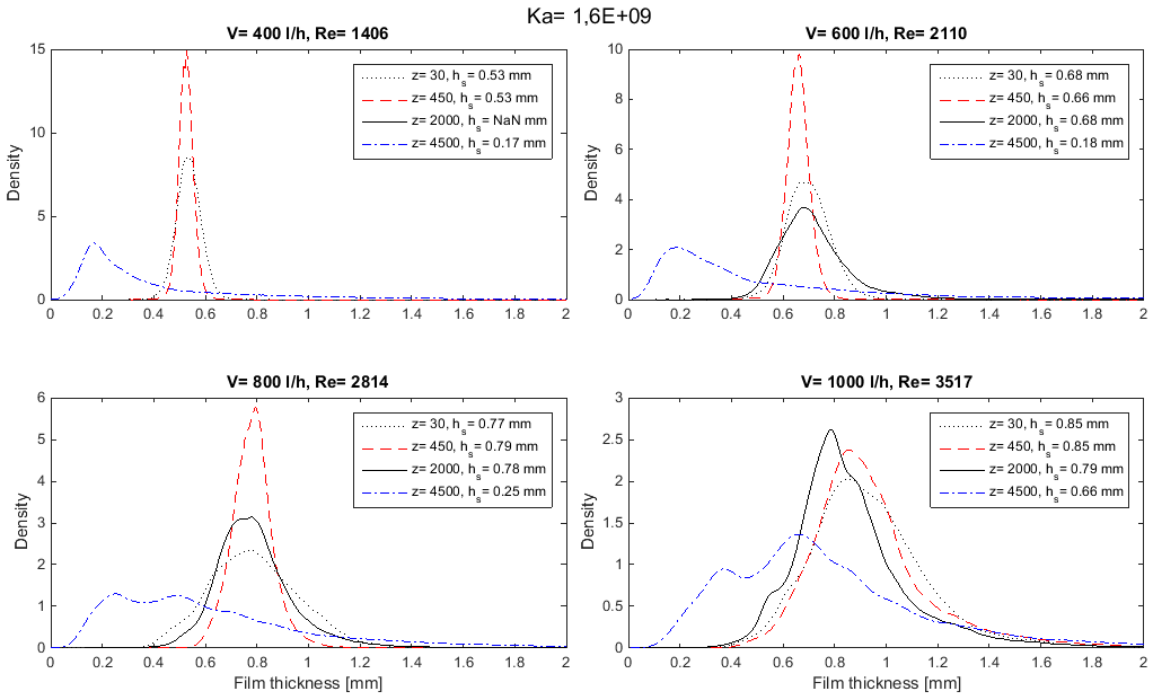

Figure 7.9: PDF at all positions for, $Ka \cong 1{,}6 \cdot 10^9$ for different Re

For all volume flows the PDF at 30 mm shows a wider distribution compared to 450 mm. This may be contributed to influence of surface tension, decreasing the wave amplitudes. This has already been investigated in 7.2. Another influence may be little air bubbles which have been observed mostly at the distributor getting less downstream.

Up to a volume flow of 600 l/h at 450 mm the PDF still shows a sharp peak with symmetrical distribution around it. Roll waves haven´t started to develop yet.

At 400 l/h corresponding to a $Re = 1406$ the flow is in the inertia-wavy turbulent flow regime (Appendix *Table 11.3*). The PDF at 2 m is not presented as an error occurred. The shape of the PDF can be estimated between 300 l/h and 500 l/h seen in an additional PDF in Appendix 11.5. Wave formation starts downstream of 450 mm, wave interaction takes place resulting in a decay of the wave crest and further transform into large liquid of lumps at 4,5 m. The large liquid lumps for 400 l/h and 600 l/h thin h_s from 0,53 mm to 0,17 mm and 0,67 mm to 0,18 mm respectively.

The mean large wave amplitudes presented later show a value of around 2 mm, thus around 10 times the substrate thickness. The pictures taken during the experiment in *Figure 7.10* show the development of the flow at 400 l/h at all four distances.

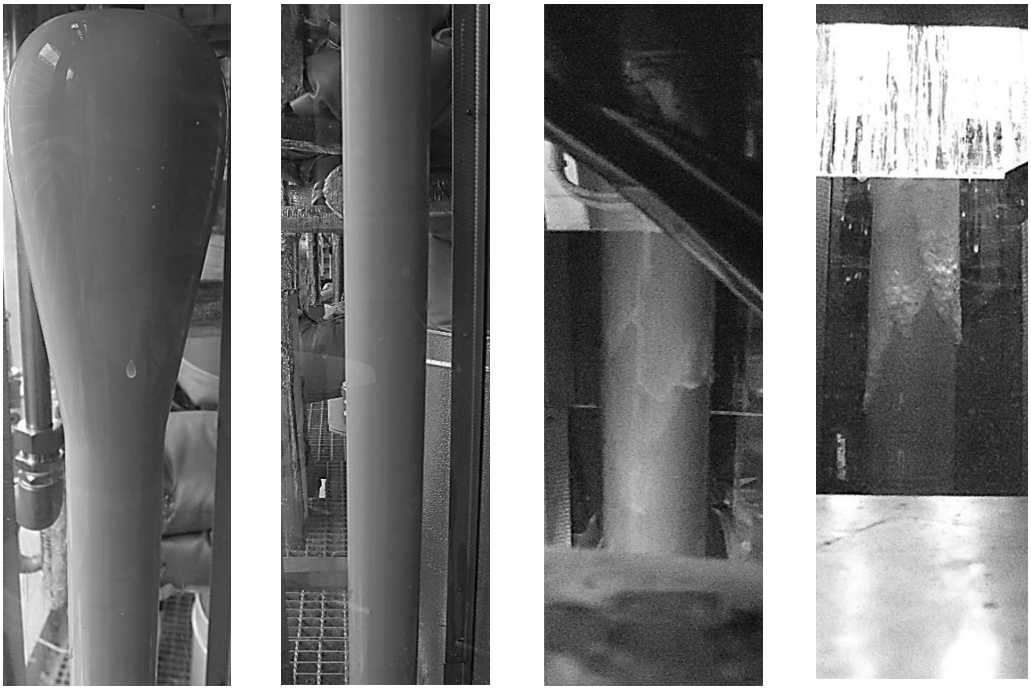

Figure 7.10: Flow development at 400l/h (Re=1406) for Ka=$1{,}6 \cdot 10^9$ *at distance of 30 mm, 450 mm, 2000 mm and 4500 mm (from left to the right).*

There it can be well seen that at 30 mm and 450 mm the surface of the film is smooth without observable waves. At 2 m small waves start to form turning into large liquid lumps at a position of 4,5 m with the thin smooth film substrate in between.

With an increase to 800 l/h ($Re = 2815$) an significant change in the PDF at 4,5 m can be observed. Two low pronounced peaks occur. The peak on the left may still correspond to large liquids of lumps travelling down and thinning the substrate. The second peak may be related to a decay of the wave crest of the large wave amplitudes. This effect further increases to 1000 l/h. Large liquid lumps still exist presented by the peak on the left and a high skewness. However turbulence start to overweight as the second peak moves to a higher value around 0,65 mm and the density of that peak increases. getting closer to $\bar{h} = 0{,}81$ mm. The turbulent flow couldn´t fully develop within this distance of pipe inlet as still waves with large amplitudes exist. In fully turbulent flow the curve will change to a Gaussian normal distribution with h_s having the same value as $\bar{h}$ of 0,81 mm. These flow pattern are pictured in *Figure 7.11*.

.

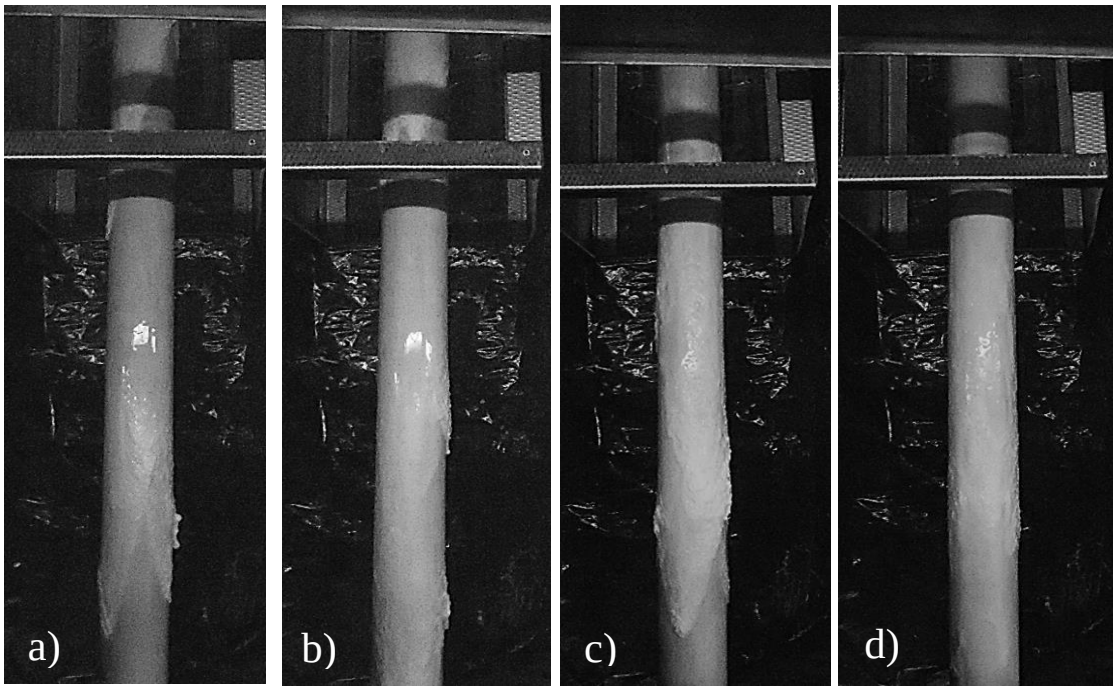

Figure 7.11: Flow pattern for Re=2815 in a) and b) and Re=3517 in c) and d) for $Ka=1{,}6 \cdot 10^9$ *at 4,5 m distance from liquid inception.*

The pictures in a) and b) of *Figure 7.11* correspond to a $Re = 2815$, c) and d) to $Re = 3517$. In a) the thin substrate between liquid lumps can be observed (left peak in PDF). In b) the flow seems more turbulent without a bigger observable liquid of lump which may be the reason for the second peak around 0,5 mm. In c) at $Re = 3517$ the liquid lumps still exist but the density decreases (left peak in the PDF). However regimes with turbulent flow seem to overweight now where no lump in d) can be seen and present the second peak at around 0,66 mm with a higher frequency.

7.4 Substrate thickness

In the following the results for the substrate thickness for both Ka over Re are presented in *Figure 7.12*. As the substrate thickness has already been referred to in recent chapters only a short description is given.

Substrate thickness for high Ka (*Figure 7.12* red right)

At 30 mm and 450 mm, h_s has almost the same values as $\bar{h}$ over the whole range of Re. Roll waves haven´t started to develop.

At 4,5 m h_s between $Re = 700 - 2200$ stays approximately constant between 0,16-0,18 mm. This concludes that the large waves have reached their maximum at 4,5 m. The minimum thinning in h_s is thus around 0,17 mm. The flow may be fully developed. The transition to fully turbulent can be seen by a further increase in Re around 2500.

h_s increases due to decay in the wave crests to a maximum $h_s = 0{,}66\,mm$. The mean film thickness $\bar{h}$ at this properties has a value of 0,81 mm. Fully turbulent flow is not given.

The influence of the roll waves is less at 2 m as they have lower amplitudes. The trend shows a damped increase of $\bar{h}$.

Substrate thickness for low Ka (*Figure 7.12* black left)

At 30 mm up to $Re = 658$, h_s has almost the same value as $\bar{h}$. With further increase in Re waves start to develop and thinning of h_s takes place.

At 450 mm up to $Re = 66$, h_s is the same as $\bar{h}$, then decreases due to the change of the capillary-wavy-laminar into the inertia-wavy-laminar flow regime. At $Re = 473$ the decay in wave crest reaches its maxima as h_s increases to values similar to $\bar{h}$. At $Re = 750$, h_s decreases again as point of strengthened wave collision may move downstream of 450 mm.

At 2 m and 4,5 m a transition is not expected. The increase in h_s is damped compared to $\bar{h}$ due to occurrence of roll-waves. Between $Re = 200 - 600$ the flow seem to be fully developed as h_s stays approximately between 0,7 – 0,8 mm.

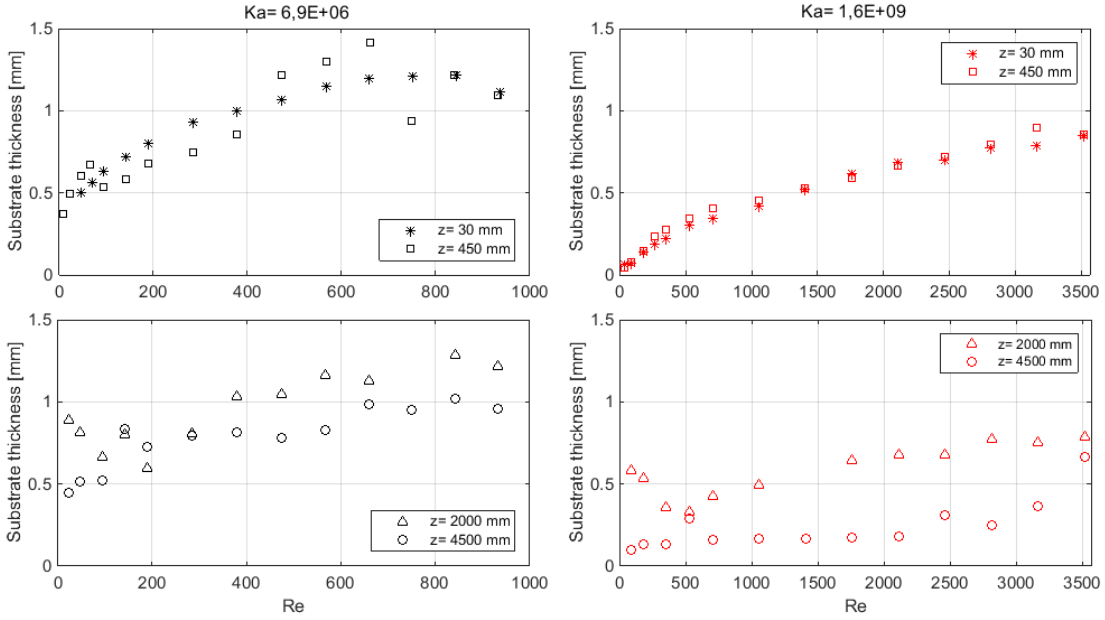

Figure 7.12: Substrate thickness h_s against Re at different laser position for $Ka = 6{,}9 \cdot 10^6$ (black, left) and $Ka = 1{,}6 \cdot 10^9$(red, right)

7.5 Wave amplitude

In this section the results of the wave amplitudes are given. *Figure 7.13* shows the total mean wave amplitude $\bar{A}$, *Figure 7.14* shows the mean wave amplitude of the Large waves $\bar{A}_L$.

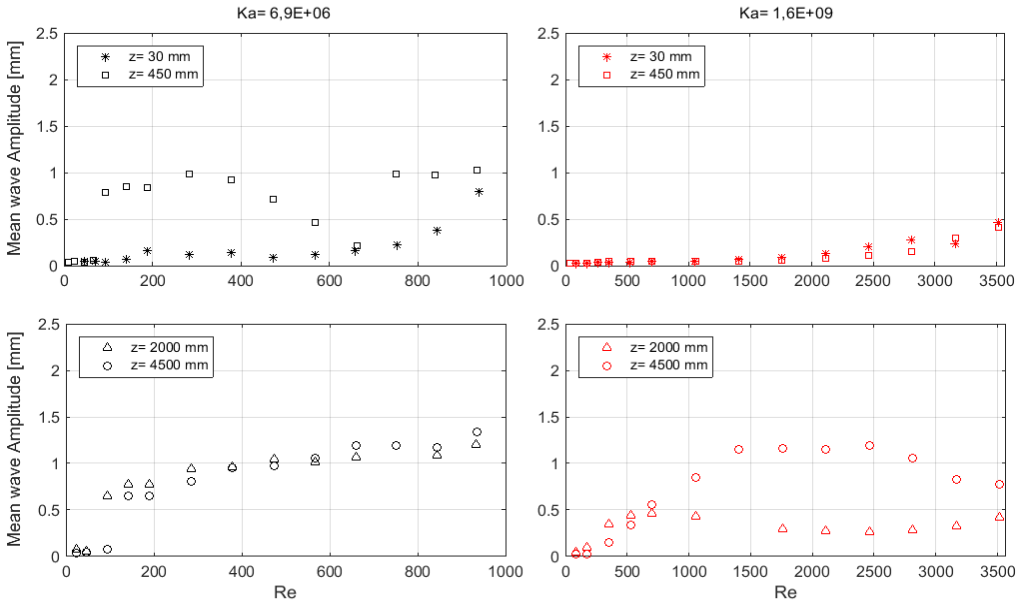

Figure 7.13: Total mean wave amplitude $\bar{A}$ against Re at different laser position for $\overline{Ka} = 6{,}9 \cdot 10^6$ (black, left) and $\overline{Ka} = 1{,}6 \cdot 10^9$(red, right)

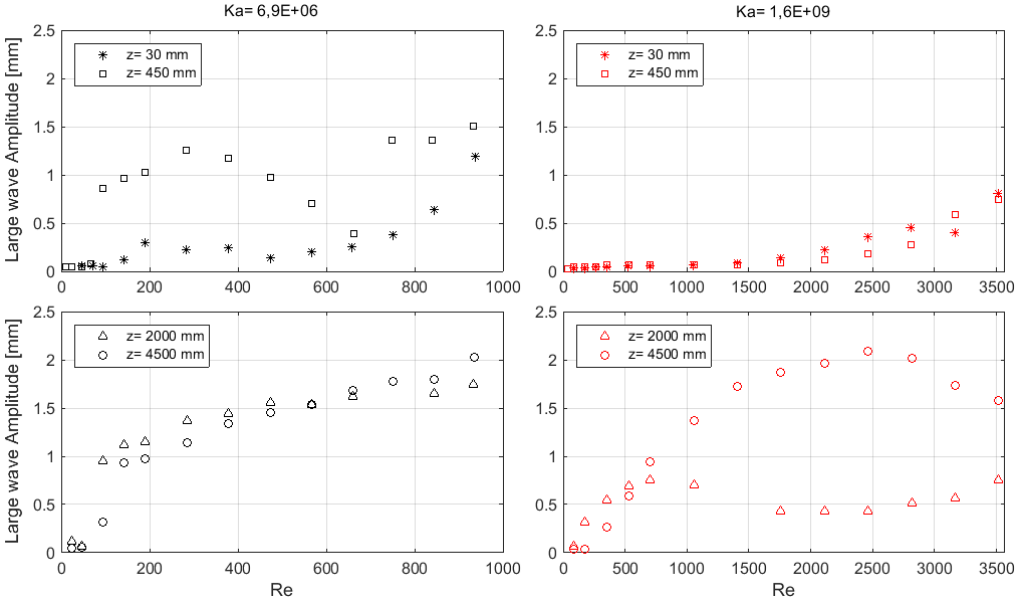

Figure 7.14: Mean Large wave amplitude $\bar{A}_L$ against Re at different laser position for $\overline{Ka} = 6{,}9 \cdot 10^6$ (black, left) and $\overline{Ka} = 1{,}6 \cdot 10^9$(red, right)

Wave amplitude for low Ka (*Figure 7.13* and *Figure 7.14*, black, left)

At 450 mm between Re=66-95 the transition to inertia-wavy-laminar flow regime takes place. $\bar{A}$ and $\bar{A}_L$ increase by 0,72 mm and 0,78 mm respectively. As the difference between these two A is quiet less it can be assumed that the most frequent roll wave with $A = \bar{A}$ arise. The film thickness trace in *Figure 7.6* agree with that. The following peak and decrease in A due to strengthened wave interaction can better be seen in *Figure 7.14* for $\bar{A}_L$. A film thickness trace due to this is presented in Appendix 11.7.

At Re > 660 the development of bigger roll waves starts already before a distance of 30 mm, and thus A increases. The increase in h_s gets damped then decreases. The maximum average amplitudes arise at 4,5 m with values around two times h_s.

Both figures represent only a very slight difference between 2 m and 4,5 m which indicates that fully developed flow may exist, developing somewhere downstream of 450 mm.

Wave amplitude for high Ka (*Figure 7.13* and *Figure 7.14*, red, right)

At 30 mm and 450 mm the amplification of the waves start at $Re \cong 1700$. This can be better seen by investigating $\bar{A}_L$.

At 4,5 m the mean wave amplitude $\bar{A}$ shows an increase until $Re \cong 1450$ then stays constant, whereas $\bar{A}_L$ further increase to $Re \cong 2500$. It seems like the amplification reaches their maximum. The substrate thickness h_s agrees with that and stays almost at a constant value of 0,17 mm constant. The maximum of $\bar{A}_L$ achieve values between 7 – 10 times the substrate thickness due to the occurrence of large liquid of lumps.

Compared to the low Ka the difference between 2 m and 4,5 m is much larger, and a statement about stable wavy flow cannot be made.

In comparison it can be seen that the behaviour of the Std as well as the mean wave amplitude $\bar{A}$ are following the behaviour of $\bar{A}_L$. The transitions are much more pronounced by investigating$\bar{A}_L$.

7.6 Wave velocity

In *Figure 7.15* the mean wave velocity u is shown. On the left side for the low $\overline{Ka}$ and on the right side for high $\overline{Ka}$. The wave velocity is highly dependent on the points between which the cross-correlation is applied and also still shows high fluctuations in between. In this figure the mean velocities u of the large waves are presented. As the cross-correlation compares two signals and calculates the lag, i.e. the time between the two maxima, this mean represents the mean velocity of the large waves and not the mean of all waves. It is possible to recognize the similarity between the wave amplitude of the large waves in *Figure 7.14* and u. It increases due to an increase in Re as the mean film velocity increases, which is related to $\bar{h}$. However, u mostly increases due to an increase in wave amplitude.

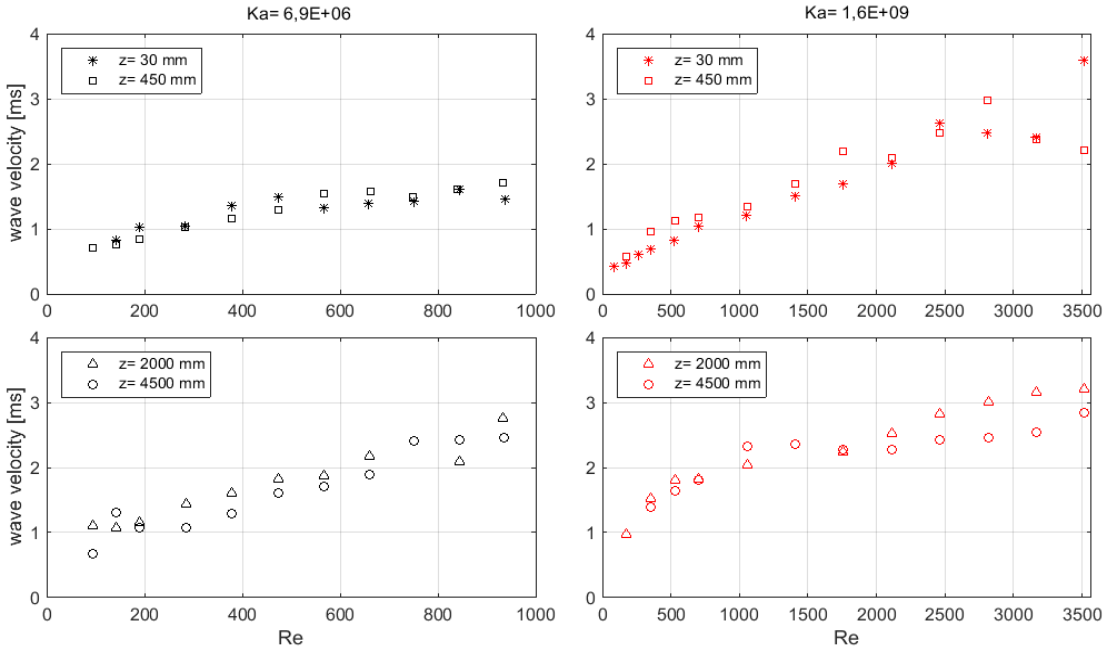

Figure 7.15: Wave velocity at against Re at different laser position for $\overline{Ka} = 6{,}9 \cdot 10^6$ *(black, left) and* $\overline{Ka} = 1{,}6 \cdot 10^9$*(red, right)*

For both $\overline{Ka}$ at the lower distances at 30 mm and 450 mm u shows an increase similar to the results for $\bar{h}$. This is due to the fact the waves start to develop in the region between liquid inception and a distance of 450 mm but are still small compared with distances further downstream at a position of 2 m and 4,5 m. Thus the increase in u in this region is mostly related to $\bar{h}$ and thus the velocity of the film substrate. For the high Ka at 30 mm and 450 mm and $Re > 3000$ the behaviour is strange which may be related to an inaccuracy of the method applied respectively that the signal cross correlation has difficulties to find the right signal similiarities.

At a distance of 450 mm for the low $\overline{Ka}$, u stays almost constant. This is related to decrease in wave amplitude by decay in wave crest which follows a decrease in u. The velocity does not follow directly the profile of the wave amplitude as the velocity of the film still increases and thus damps the effect. In the region where $\bar{A}_L$ increase again, also u increases. The same effect is seen from the transition between the inertia-wavy-laminar and inertia-wavy turbulent flow regime at a $\overline{Ka}$=$1{,}6 \cdot 10^9$ at a distance of 4,5 m. At $\overline{Ka}$=$6{,}9 \cdot 10^6$ at a distance of 2 m and 4,5 m u follows the increase of the profile of the large waves amplitudes. The increase shows linear behaviour.

7.7 Wave frequency

In the following a selection of frequencies related to the investigated transitions are given in the following two figures. *Figure 7.16* shows frequencies for the high Ka and *Figure 7.17* for the low Ka. Y(t) represents h(t) which gets transformed into the frequency domain thus Y(f). |Y(f)| represent the magnitude of the corresponding frequency.

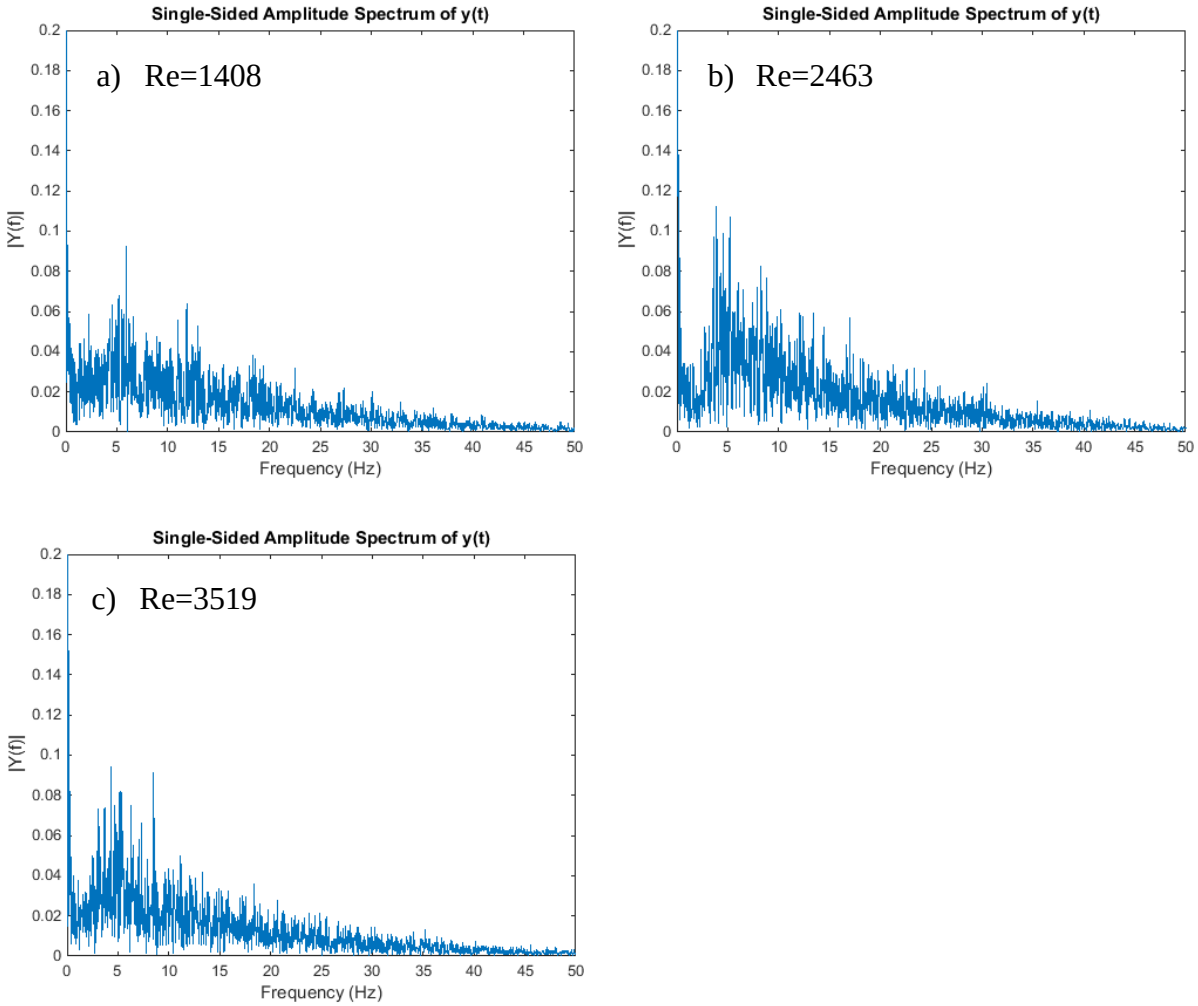

Figure 7.16: Selection of single-sided Ampliude spectrum at 450 mm for $\overline{Ka} = 1{,}6 \cdot 10^9$ *and different Re.*

In *Figure 7.16*, *A* increases from $Re = 1408 - 2463$ followed by the decay in the wave crest, starting after $Re = 2463$. The magnitude |Y(f)| follows the behaviour of A. The frequency between a) and b) gets slightly reduced from around 6 to 4 *Hz.* This may be related to the large liquid lumps with a lower frequency. At $Re = 3519$ the flow pattern get more turbulent with frequencies between 4 – 10 *Hz.*

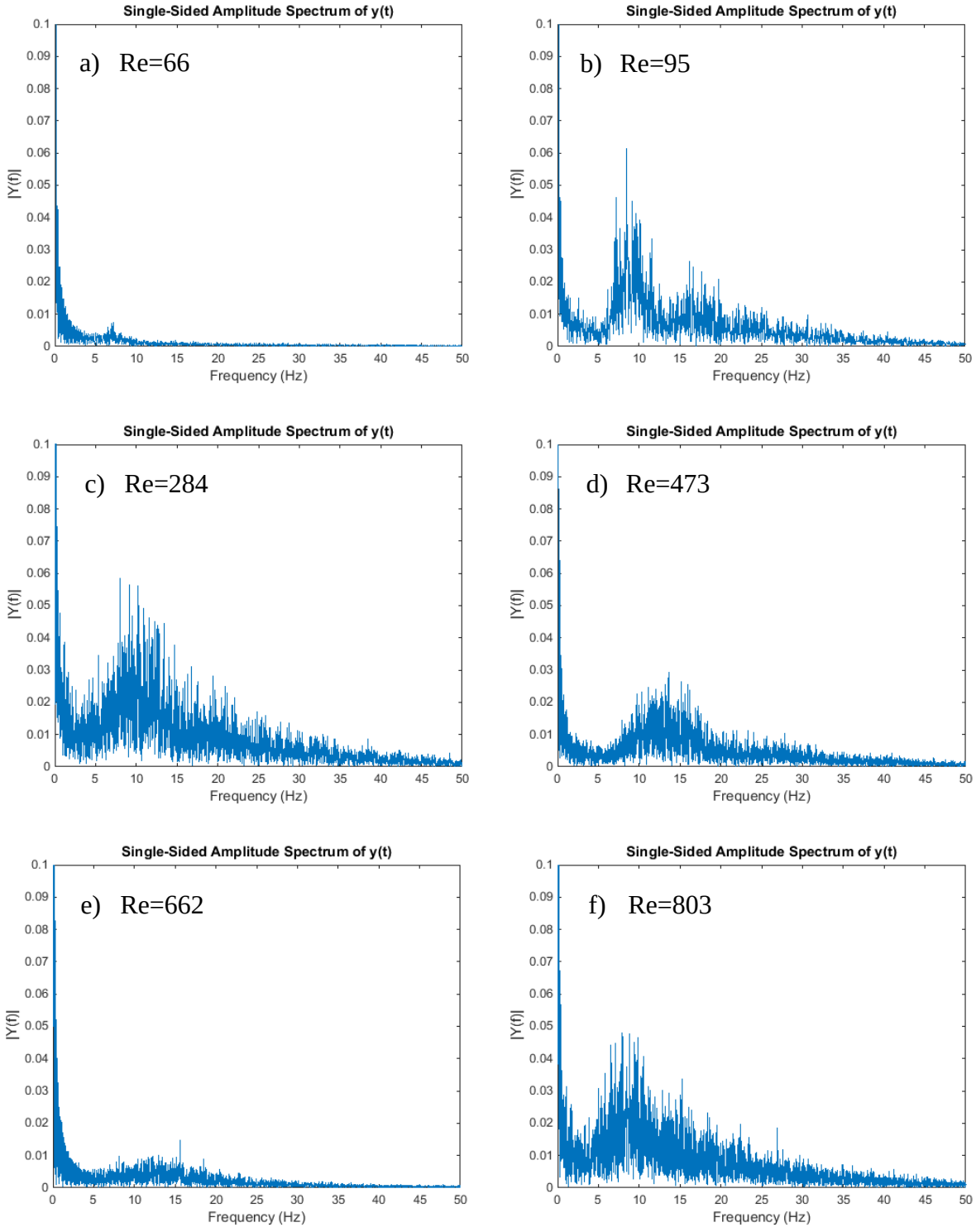

Figure 7.17: Selection of single-sided Ampliude spectrum at 450 mm for $\overline{Ka} = 6{,}9 \cdot 10^6$ *and different Re.*

In *Figure 7.17* in a) and b) the transition from the capillary-wavy-laminar to the inertia-wavy-laminar flow is presented. The frequency f of the capillary-waves is around 7. After the transition the magnitude increases due to increase in A. The frequency of the roll waves is between 7-10, which can also be investigated by looking at the film thickness traces represented in *Figure 7.6*. The figure c) – f) show the decay in the wave crest. In c) A have reached their maximum. The most common f are between $8 - 12\ Hz$. The increases in Re follows roll waves with higher frequencies. With a further increase the magnitude gets less and moves to higher frequencies between 10-17, whereas the maximum in decay in the wave crest is reached at $Re = 662$. At this point it is difficult to investigate a range of most common frequencies. The flow shows fully turbulent flow pattern. The substrate thickness h_s has reached the same value as $\bar{h}$. In f) for $Re = 803$ it represents the point where the wave collision may move downstream of 450 mm. Roll waves occur again with $f = 7 - 10\ Hz$.

8 Conclusion

The new laser measurement approach gives highly resolved film thickness traces. This is especially helpful to investigate the transitions between the flow regimes as well as to identify the behaviour of different parameters. The most promising parameter to identify flow regimes respectively the transition between them, are the mean film thickness $\bar{h}$, the substrate film thickness h_s, and the wave amplitude A.

The mean film thickness is very helpful for the validation of the results by comparing them to results from previous publications as well as film thickness correlations. Further it gives information about the validity of the measurements to investigate the longitudinal flow development. $\bar{h}$ should decrease downstream due to increase in velocity. Even though it has also been investigated a thinner $\bar{h}$ at 30 mm from fluid inception compared to 450 mm from fluid inception. This may be related to the development of roll waves at 30 mm picking up liquid at the wave through, which result in a thinner $\bar{h}$ (film thinning by roll waves).

The result of $\bar{h}$ for the high viscosity are very good compared to the film thickness correlations of Nusselt for laminar and from Lukach for wavy-laminar-flow. For the low viscosity $\bar{h}$ follows the trend of Lukach with a difference of approximately 0,2 mm.

The substrate film thickness h_s is determined by applying the probability density function and referred to as the most frequent film thickness. Compared with $\bar{h}$ it gives information about the wave development, thus the amplification as well as decay in the wave crest and thus information about the transitions. For purely laminar flow h_s is identical to $\bar{h}$. They differ as roll waves occur, thinning the substrate. In a total decay in the wave crest thus with fully turbulent flow pattern they are the same again. A real "substrate" only exist in the inertia-wavy-laminar and inertia-wavy-turbulent flow regime not in the purely laminar, wavy-capillary-laminar as well as fully turbulent flow regime.

The new method developed to distinguish between different wave amplitudes shows more pronounced results to identify the transitions compared to the standard deviation and further gives information about the magnitude of the amplitudes.

The Reynolds numbers investigated for $\overline{Ka} = 6{,}9 \cdot 10^6$ (high viscosity) are Re up to around 1000 and for $\overline{Ka} = 1{,}6 \cdot 10^9$ (low viscosity) Re up to around 3500.

The critical Reynolds number according to Al-Sibai, 2004 for the beginning of fully turbulent flow show a value of 2735 for the high Ka. This value is defined by a reduction in wave amplitudes due to strengthened wave collision/ interaction. For the low viscosity the investigated value for the critical Reynold number is similar and between $Re \cong 2500 - 2800$. Fully turbulent flow could however not be investigated also at $Re = 3500$ and a distance of 4,5 m from fluid inception. At these conditions large liquid lumps with a thin substrate in between ($\cong 0{,}2\ mm$) still exist. The maximum average amplitudes of these large liquid lumps showed values around 7-10 times the substrate thickness.

Although the range of Re investigated is not high enough to observe fully turbulent flow, local fully turbulent flow pattern can exist at much lower Re. For the high viscosity at 450 mm and $Re \cong 700$, a total decay in wave amplitude occurred. The value of h_s reached the same value as $\bar{h}$. At these position and conditions the flow

pattern are fully turbulent. Downstream of 450 mm however waves start again to develop. Therefore the flow pattern can be fully turbulent locally although the whole flow is not fully turbulent.

Fully developed flow could be determined for the low viscosity at a position of 4,5 m, developing between 2 – 4,5 m. For the high viscosity the flow may already be fully developed at a distance of 2 m, developing between 450 mm and 2 m. The flow therefore needs a shorter length to get fully developed for the higher viscosity. The development of waves start closer to fluid inception for the high viscosity at 450 mm whereas for the low viscosity waves start to develop around 2 m distance from fluid inception.

The transitions from the capillary-wavy-laminar into the inertia-wavy-laminar flow regime has been determined for the high viscosity at 450 mm from fluid inception for $Re \cong 66 - 95$. Ishigai et al., 1972 reported a value of $Re = 43$ and Al-Sibai, 2004 a value of $Re = 19$, both depending on Ka. A further transition into the inertia-wavy-turbulent regime may occur around 4,5 m from fluid inception at $Re \cong 189$. This value is lower than represented by Ishigai et al., 1972 ($Re \cong 300$) and Al-Sibai $Re \cong 400$. Ishigai investigated the flow pattern on the outside of a tube at 2 m distance from fluid inception, whereas Al-Sibai investigated the flow pattern on a flat plate at a position of approximately 1,1 m from fluid inception. Ishigai reported that a length of two meter may not be long enough to give a true value for a critical Reynolds number Re_{crit} (Ishigai et al., 1972). The results presented here show that Re_{crit} is highly dependent on the position it is determined. The transition into inertia-wavy turbulent flow regime takes place for a lower Re as it is investigated at 4,5 m whereas the transition to inertia-wavy-laminar flow regime takes place at $Re \cong 66 - 95$. The latter is higher in comparison to Ishigai and Al-Sibai as it has been investigated at a closer distance to fluid inception.

The investigations of the transition regimes have been limited to volume flows > 200 l/h for distances downstream of 450 mm. The pipe was slightly bended in the middle around two meters, which highly influenced the results, leading to uneven liquid distribution and wetting problems. Dry outs occurred at volume flows below 100 l/h. The influence gets less above 200 l/h. The effect is lower for a lower Ka as the development of roll waves start earlier as for higher Ka. When roll waves appear, their main forces are inertia and gravity which are overweighting compared to the driving force of the liquid following the bended pipe.

In conclusion it can be said that the critical Reynolds numbers are highly depended on the longitudinal distance from fluid inception as well as of Ka, which leads to different Re_{crit} reported by different authors. Fully turbulent low pattern can occur for much lower values than Re_{crit} describing the transition into fully turbulent flow. The transitions in the flow pattern are highly related to the largest waves. For volume flows below 200 l/h and a pipe length of 5 m it has to be ensured that the pipe is completely straight to prevent wetting problems. For longer pipe length this effect may be even stronger.

The result of this thesis give a valuable contribution to the understanding of liquid flow pattern of a falling liquid film.

9 Outlook

To transfer the results of uneven liquid distribution to the industry, it may be interesting to investigate the liquid distribution, where pipes with a length of or higher than five meter as well as volume flows below 200 l/h are used.

The flow development between a position of 30 mm and 450 mm is mostly quiet clear. However, between 450 mm and a position approximately at 2 m the investigation of flow pattern development is not always completely clear. The distance between these two positions is very high and the flow pattern change a lot in between. Therefore it would be interesting to extend the results with at least one additional measurement position in between these positions.

The methods applied to investigate the liquid flow pattern show interesting characteristics and good results compared to the literature. As heat transfer is highly related to the hydrodynamics it would be interesting to apply similar methods by using a pipe with a structured surface.

That the critical Reynold´s numbers are also depended on Ka has already been investigated. However it would also be interesting to gain information about the influence of different pipe diameters on the transitions.

In the literature the transition into the fully turbulent flow, shows the biggest differences in critical Reynold numbers. Therefore it would be interesting to investigate especially this transition in more detail. By investigated different solid contents and a higher range of Re a correlation dependent on Ka can be determined.

10 References

Adomeit, P., Renz, U., 2000. Hydrodynamics of three-dimensional waves in laminar falling films. Int. J. Multiph. Flow 26, 1183–1208. doi:10.1016/S0301-9322(99)00079-8

Akesjö, A., Olausson, L., Vamling, L., Gourdon, M., 2015. New measurement approaches for film thickness and wall temperature in falling film heat exchangers.

Alhusseini, A.A., Chen, J.C., 2000. Transport Phenomena in Turbulent Falling Films. Ind. Eng. Chem. Res. 39, 2091–2100. doi:10.1021/ie9906013

Alhusseini, A.A., Tuzla, K., Chen, J.C., 1998. Falling film evaporation of single component liquids. Int. J. Heat Mass Transf. 41, 1623–1632. doi:10.1016/S0017-9310(97)00308-6

Al-Sibai, F., 2004. Experimentelle Untersuchung der Strömungscharakteristik und des Wärmeübergangs bei welligen Rieselfilmen. Technische Hochschule Aachen, Aachen.

Aviles, M.L., 2007. Experiments on falling film evaporation of a water-ethylene glycol mixture on a surface with longitudal grooves. Technische Universität Berlin, Berlin.

Bandelier, P., 1997. Improvement of multifunctional heat exchangers applied in industrial processes. Appl. Therm. Eng. 17, 777–788. doi:10.1016/S1359-4311(97)00010-0

Bird, R.B., Stewart, W.E., Lightfoot, E.N., 2007. Transport Phenomena. John Wiley & Sons.

Brauner, N., 1989. Modelling of wavy flow in turbulent free falling films. Int. J. Multiph. Flow 15, 505–520. doi:10.1016/0301-9322(89)90050-5

Brauner, N., 1987. Roll wave celerity and average film thickness in turbulent wavy film flow. Chem. Eng. Sci. 42, 265–273. doi:10.1016/0009-2509(87)85056-X

Brauner, N., Maron, D.M., 1982. Characteristics of inclined thin films, waviness and the associated mass transfer. Int. J. Heat Mass Transf. 25, 99–110. doi:10.1016/0017-9310(82)90238-1

Chu, K.J., Dukler, A.E., 1975. Statistical characteristics of thin, wavy films III. Structure of the large waves and their resistance to gas flow. AIChE J. 21, 583–593. doi:10.1002/aic.690210323

Chu, K.J., Dukler, A.E., 1974. Statistical characteristics of thin, wavy films: Part II. Studies of the substrate and its wave structure. AIChE J. 20, 695–706. doi:10.1002/aic.690200410

Chun, K.R., Seban, R.A., 1971. Heat Transfer to Evaporating Liquid Films. J. Heat Transf. 93, 391–396. doi:10.1115/1.3449836

Dietze, G.F., Al-Sibai, F., Kneer, R., 2009. Experimental study of flow separation in laminar falling liquid films. J. Fluid Mech. 637, 73–104.

Dietze, G.F., Leefken, A., Kneer, R., 2008. Investigation of the backflow phenomenon in falling liquid films. J. Fluid Mech. 595, 435–459. doi:10.1017/S0022112007009378

Doro, E.O., 2012. Computational modeling of falling liquid film free surface evaporation. Georgia Institute of Technology.

Drosos, E.I.P., Paras, S.V., Karabelas, A.J., 2004. Characteristics of developing free falling films at intermediate Reynolds and high Kapitza numbers. Int. J. Multiph. Flow 30, 853–876.

Fulford, G.D., 1964. The Flow of Liquids in Thin Films, in: Advances in Chemical Engineering. Elsevier, pp. 151–236.

Ishigai, S., Nakanisi, S., Koizumi, T., Oyabu, Z., 1972. Hydrodynamics and Heat Transfer of Vertical Falling Liquid Films : Part 1, Classification of Flow Regimes. Bull. JSME 15, 594–602. doi:10.1299/jsme1958.15.594

Johansson, M., 2008. Heat Transfer and Hydrodynamics in Falling Film Evaporation of Black Liquor (Doctoral thesis). Chalmers University of Technology.

Karapantsios, T.D., Paras, S. t, Karabelas, A.J., 1989. Statistical characteristics of free falling films at high Reynolds numbers. Int. J. Multiph. Flow 15, 1–21.

Karimi, G., Kawaji, M., 1999. Flow characteristics and circulatory motion in wavy falling films with and without counter-current gas flow. Int. J. Multiph. Flow 25, 1305–1319. doi:10.1016/S0301-9322(99)00044-0

Kil, S.H., Kim, S.S., Lee, S.K., 2001. Wave characteristics of falling liquid film on a vertical circular tube. Int. J. Refrig. 24, 500–509.

Kostoglou, M., Samaras, K., Karapantsios, T.D., 2010. Large wave characteristics and their downstream evolution at high Reynolds number falling films. AIChE J. 56, 11–23. doi:10.1002/aic.11992

Kunugi, T., Kino, C., 2005. DNS of falling film structure and heat transfer via MARS method. Comput. Struct., Frontier of Multi-Phase Flow Analysis and Fluid-Structure Frontier of Multi-Phase Flow Analysis and Fluid-Structure 83, 455–462. doi:10.1016/j.compstruc.2004.08.018

Mascarenhas, N., Mudawar, I., 2014. Statistical analysis of measured and computed thickness and interfacial temperature of free-falling turbulent liquid films. Int. J. Heat Mass Transf. 73, 716–730. doi:10.1016/j.ijheatmasstransfer.2014.02.054

Micro-Epsilon. Laser-Scanner Manual. [WWW Document], n.d. URL http://www.micro-epsilon.com/download/manuals/man--scanCONTROL-29xx--en.pdf (accessed 3.5.15).

Miller, W.A., Keyhani, M., n.d. The effect of roll waves on the hydrodynamics of falling films observed in vertical column aborbers.

Paras, S.V., Karabelas, A.J., 1991. Properties of the liquid layer in horizontal annular flow. Int. J. Multiph. Flow 17, 439–454. doi:10.1016/0301-9322(91)90041-Z

Patnaik, V., Perez-Blanco, H., 1996a. Roll waves in falling films: an approximate treatment of the velocity field. Int. J. Heat Fluid Flow 17, 63–70.

Patnaik, V., Perez-Blanco, H., 1996b. Roll waves in falling films: an approximate treatment of the velocity field. Int. J. Heat Fluid Flow 17, 63–70. doi:10.1016/0142-727X(95)00075-2

Salazar, R.P., Marschall, E., 1978. Time-average local thickness measurement in falling liquid film flow. Int. J. Multiph. Flow 4, 405–412. doi:10.1016/0301-9322(78)90034-4

Takahama, H., Kato, S., 1980. Longitudinal flow characteristics of vertically falling liquid films without concurrent gas flow. Int. J. Multiph. Flow 6, 203–215. doi:10.1016/0301-9322(80)90011-7

Telles, A.S., Dukler, A.E., 1970. Statistical Characteristics of Thin, Vertical, Wavy, Liquid Films. Ind. Eng. Chem. Fundam. 9, 412–421. doi:10.1021/i160035a018

Wasden, F.K., Dukler, A.E., 1989. Insights into the hydrodynamics of free falling wavy films. AIChE J. 35, 187–195. doi:10.1002/aic.690350203

Weise, F., Scholl, S., 2007. Evaporation of pure liquids with increased viscosity in a falling film evaporator. Heat Mass Transf. 45, 1037–1046. doi:10.1007/s00231-007-0317-9

Zadrazil, I., Matar, O.K., Markides, C.N., 2014. An experimental characterization of downwards gas–liquid annular flow by laser-induced fluorescence: Flow regimes and film statistics. Int. J. Multiph. Flow 60, 87–102. doi:10.1016/j.ijmultiphaseflow.2013.11.008

11 Appendix

11.1 Wave classification

The first classification of the waves has been done due to the location of the maxima but does not take into account the local minima. If the local minima are very close to the maxima the resulting A is as small as a substrate wave but still counts to the "bigger waves". Therefore a second classification due to wave amplitudes is defined, which three different ranges for the wave amplitudes investigated, see *Table 11.1*

Table 11.1: Second classification due to wave amplitudes: Three different ranges are investigated

Wave amplitude	**Range 1**	**Range 2**	**Range 3**
SMALL	–	$A > \frac{1}{3} * Std_h$	$A > \frac{1}{2} * Std_h$
BIG	–	$A > \frac{1}{2} * Std_h$	$A > Std_h$
LARGE	–	$A > Std_h$	$A > 1{,}5 * Std_h$

The first "Range 1" distinguish the waves only due to the maxima without taking into account the location of the minima thus also small fluctuations. With "Range 2" and "Range 3" different values for the amplitude height are tested. The results for the different ranges are shown for the experiments in *Table 11.2*. It can be seen that the differences in the mean amplitudes for the three ranges is small. However, if the amplitude of single waves are investigated, or the minimum amplitudes, then the difference is much higher. The maximum stays the same as this is already fixed by the first distinction of the maxima and has no influence. To picture the behaviour of the wave amplitudes and the change in the minima due to the three ranges investigated, a probability distribution is shown in *Figure 11.1* showing a notable change in the minima of the big wave amplitudes.

Table 11.2:Results for the Validity of wave amplitudes for the three different ranges for different experiments. Ka for all experiments approximately $Ka \cong 1{,}6 \cdot 10^9$ and a distance z of 2000 mm

Exp. Nr.	$\dot{V}$ [l/h]	$\bar{A}_{small}$ [mm]	$\bar{A}_{Big}$ [mm]	$\bar{A}_{Large}$ [mm]	$\bar{A}_{total}$ [mm]	Min/Max A_{Big} [mm]	Min/Max A_{Large} [mm]
53	600						
Range 1		0,52	0,91	1,51	0,97	0,08 / 1,68	0,00 / 2,80
Range 2		0,54	0,92	1,52	0,99	0,23 / 1,68	0,46 / 2,80
Range 3		0,56	0,95	1,54	1,02	0,45 / 1,68	0,68 / 2,80
47	200						
Range 1		0,34	0,67	1,14	0,73	0,11 / 1,18	0,45 / 2,04
Range 2		0,37	0,67	1,14	0,76	0,17 / 1,18	0,45 / 2,04
Range 3		0,39	0,69	1,15	0,78	0,32 / 1,18	0,49 / 2,04

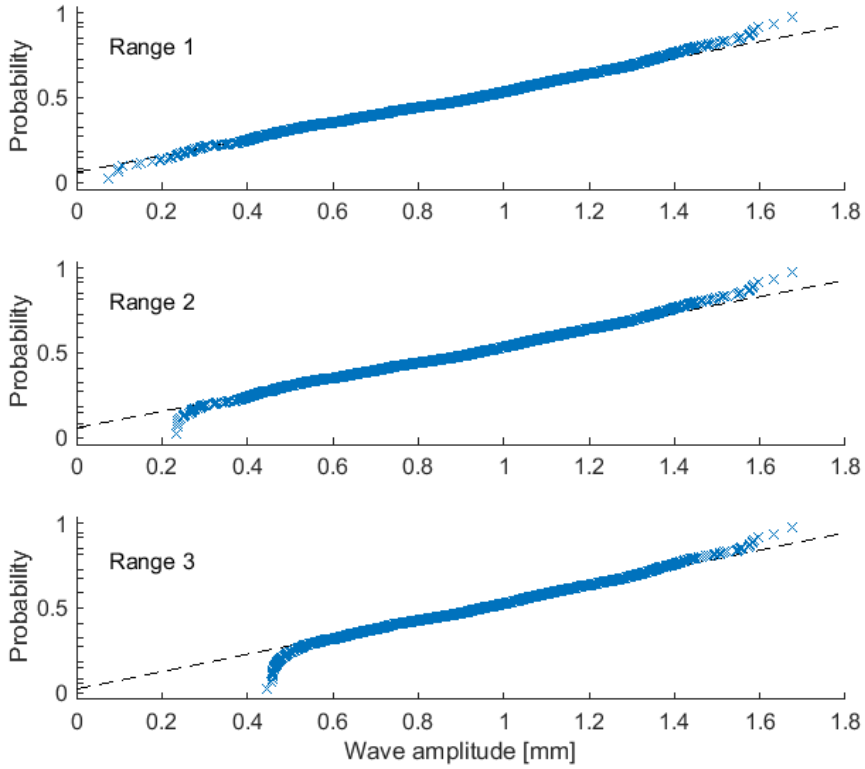

Figure 11.1: Probability distribution of big wave amplitudes for three different Ranges of wave amplitude validity for Experiment Nr. 53.

Although the different ranges have a limited influence on the mean amplitudes in the presented case, it may be higher for other experiments. Therefore range 3 is chosen and the mean wave amplitudes for all experiments are calculated according to these values.

11.2 Critical Reynold numbers recalculated

Table 11.3. Calculation of different flow regimes du to $Ka = 6{,}9 \cdot 10^6$ and $Ka = 1{,}6 \cdot 10^9$ for different references

$\boldsymbol{Ka = 1{,}6 \cdot 10^9}$	Brauer 1956 reported by Weise and Scholl, 2007	Ishigai et al., 1972	Patnaik and Perez-Blanco, 1996	Al-Sibai, 2004
Laminar	**Re4** < 16	**Re4** < 7	**Re4** < 20	**Re4** < 20
transition		7 < Re4 < 73		
Wavy laminar	16 < **Re4** < 1600	73 < **Re4** < 300	capillary wavy laminar 20 < **Re4** < 200; inertia wavy laminar 200 < **Re4** < 1000	capillary wavy laminar 20 < **Re4** < 33; inertia wavy laminar 33 < **Re4** < 672/1063
transition		300 < **Re4** < 1600	inertia wavy turbulent 1000 < **Re4** < 4000	672/1063 < **Re4** < 2735
Fully turbulent	**Re4** > 1600	**Re4** > 1600	**Re4** > 4000	**Re4** > 2735

$\boldsymbol{Ka = 6{,}9 \cdot 10^6}$	Brauer 1956 reported by Weise and Scholl, 2007	Ishigai et al., 1972	Patnaik and Perez-Blanco, 1996	Al-Sibai, 2004
Laminar	**Re4** < 16	**Re4** < 5	**Re4** < 20	**Re4** < 12
transition		5 < Re4 < 43		
Wavy laminar	16 < **Re4** < 1600	43 < **Re4** < 300	capillary wavy laminar 20 < **Re4** < 200; inertia wavy laminar 200 < **Re4** < 1000	capillary wavy laminar 12 < **Re4** < 19; inertia wavy laminar 19 < **Re4** < 413/618
transition		300 < **Re4** < 1600	inertia wavy turbulent 1000 < **Re4** < 4000	413/618 < **Re4** < 1976
Fully turbulent	**Re4** > 1600	**Re4** > 1600	**Re4** > 4000	**Re4** > 1976

11.3 Mean film thickness – additional figures

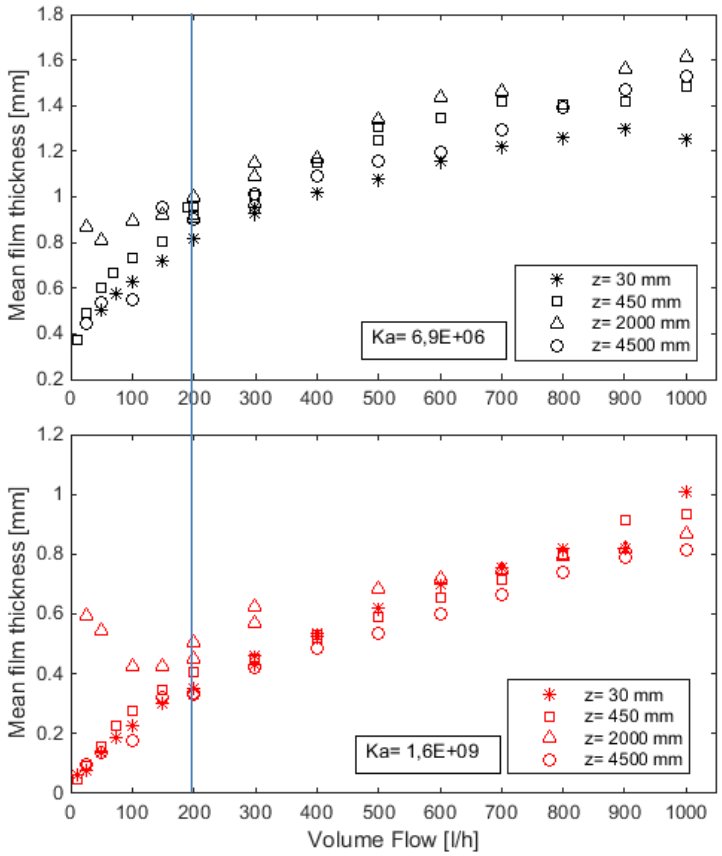

Figure 11.2: Mean film thickness against volume flow at different positions z and $\overline{Ka} = 6{,}9 \cdot 10^6$ *(black, top) and* $\overline{Ka} = 1{,}6 \cdot 10^9$*(red, bottom)*

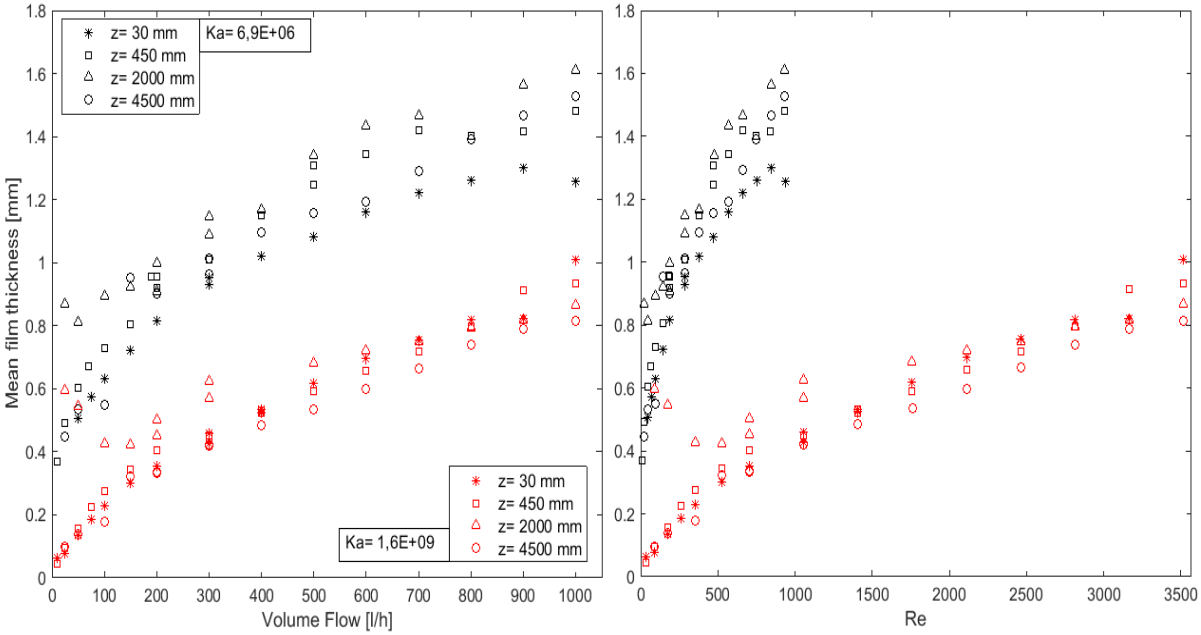

Figure 11.3: Mean film thickness against volume flow and Re for both Ka

11.4 Transition capillary-wavy-laminar to wavy-laminar

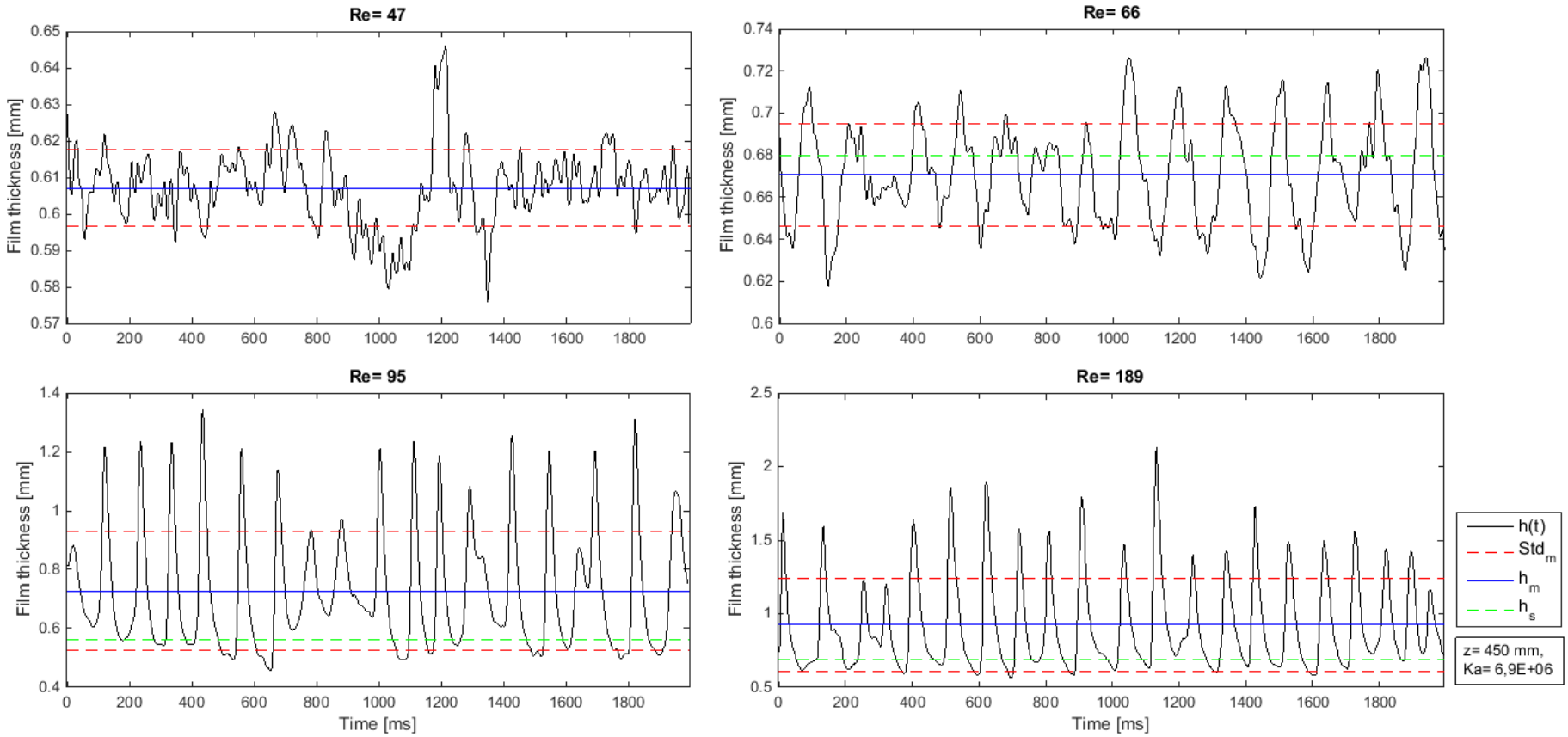

Figure 11.4: Film thickness trace at $450\ mm$, $Ka \cong 6{,}9 \cdot 10^6$ *for* Re *=47-189 corresponding to the PDF of Figure 7.5.*

The film thickness trace, in *Figure 11.4* over a measuring time range of 2000 ms shows the transition from the capillary-wavy-laminar to the inertia-wavy-laminar flow regime between $Re = 66 - 95$.

In the capillary-wavy-laminar flow regime the value for the substrate thickness is a more imaginary value, a substrate between the waves doesn´t really exist ($Re = 47 - 66$) whereas in the inertia-wavy-laminar flow regime a substrate film between the waves is clearly observable ($Re = 95 - 189$).

Table 11.4 gives further information about the maximum positive and negative film thickness fluctuation within this film thickness trace. The fluctuations are related to the substrate thickness (green line in *Figure 11.4*).

Table 11.4: Positive and negative fluctuations related to

Re	**47**	**66**	**95**	**189**
(Exp.Nr)	(94)	(93)	(92)	(90)
Fluctuation positive max [mm]	0,04	0,05	0,8	1,4
Fluctuation negative max [mm]	0,03	0,06	0,1	0,1

A capillary-wavy-laminar film has small fluctuations around the substrate thickness which is almost identical to the mean film thickness. The fluctuations are with nearly the same amplitude in both directions. With increasing Re from 47 to 66 the average fluctuations increase but it is still possible to recognize a capillary wavy flow as the fluctuations have the same value in both directions (symmetrical). With a further increase of Re from 66 to 95 the positive fluctuation rapidly increases by around 0,75 mm whereas the amplitudes with negative fluctuation increase only very slightly (0,04 mm).

The effect is clear if the mean film thickness is compared with the substrate thickness, see *Figure 11.5* The substrate thickness differs significantly after the transition region and is around 0,2 mm less than the mean film thickness. In this figure, values with lower Re are also shown but not presented in the PDF of

Figure 7.5. The transition region is marked in green.

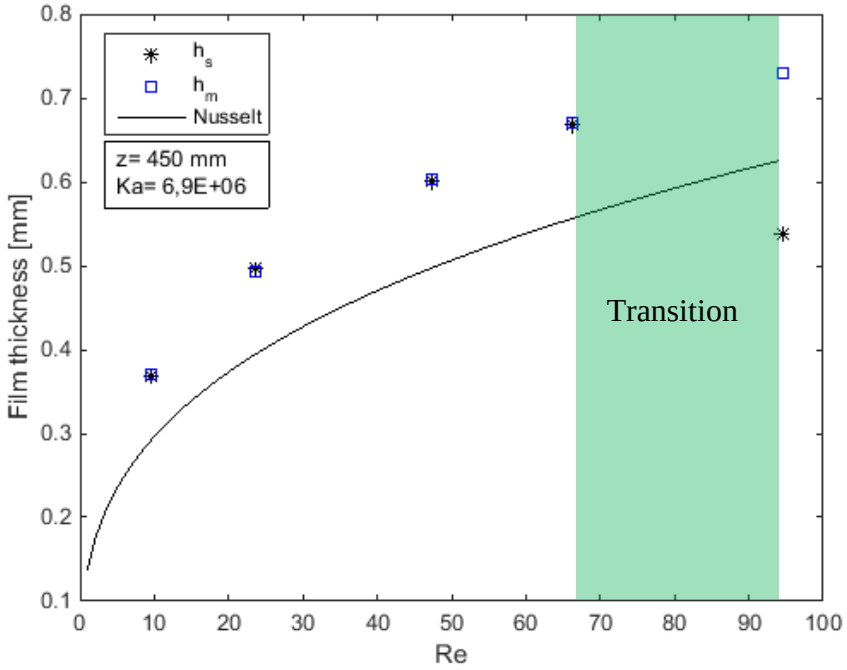

Figure 11.5: Mean film thickness h_m and substrate film thickness h_s vs Re. The expected transition from capillary-wavy laminar to inertia-wavy laminar is marked in green.

11.5 Additional PDF for high Ka

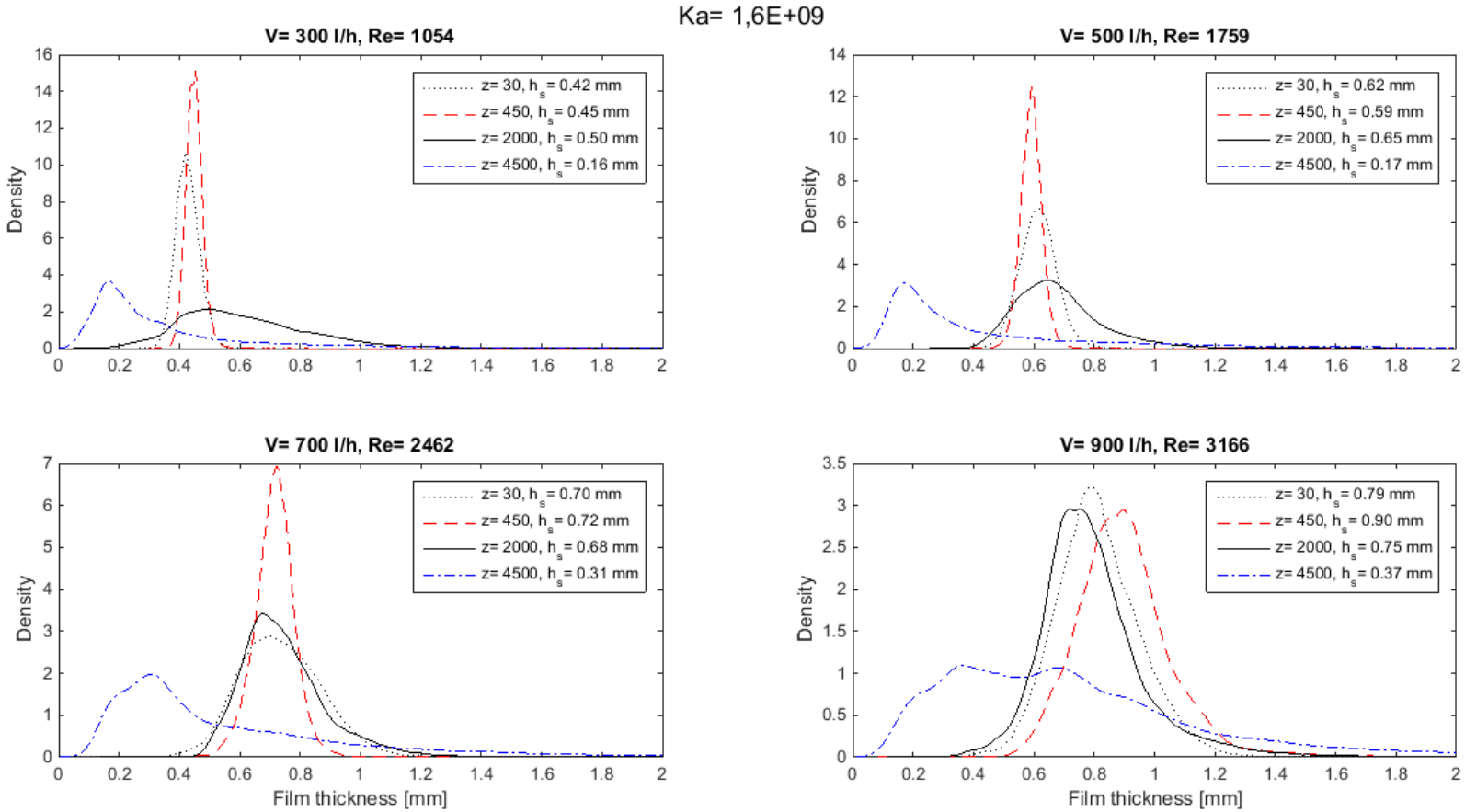

Figure 11.6: Additional PDF for $Ka \cong 1{,}6 \cdot 10^9$

11.6 PDF for high Ka at 30 mm and 450 mm for low Re

Figure 11.7 presents the PDF at 30 mm and 450 mm for the lower Re range for volume flows smaller than 400 l/h. Here in both cases the PDF still shows a symmetrical behaviour. The distribution is a bit wider at a distance of 30 mm than 450 mm due to the influence of the distributor, bubble formation and influence of surface tension. This has been mention in Chapter 7.2 and 7.3.

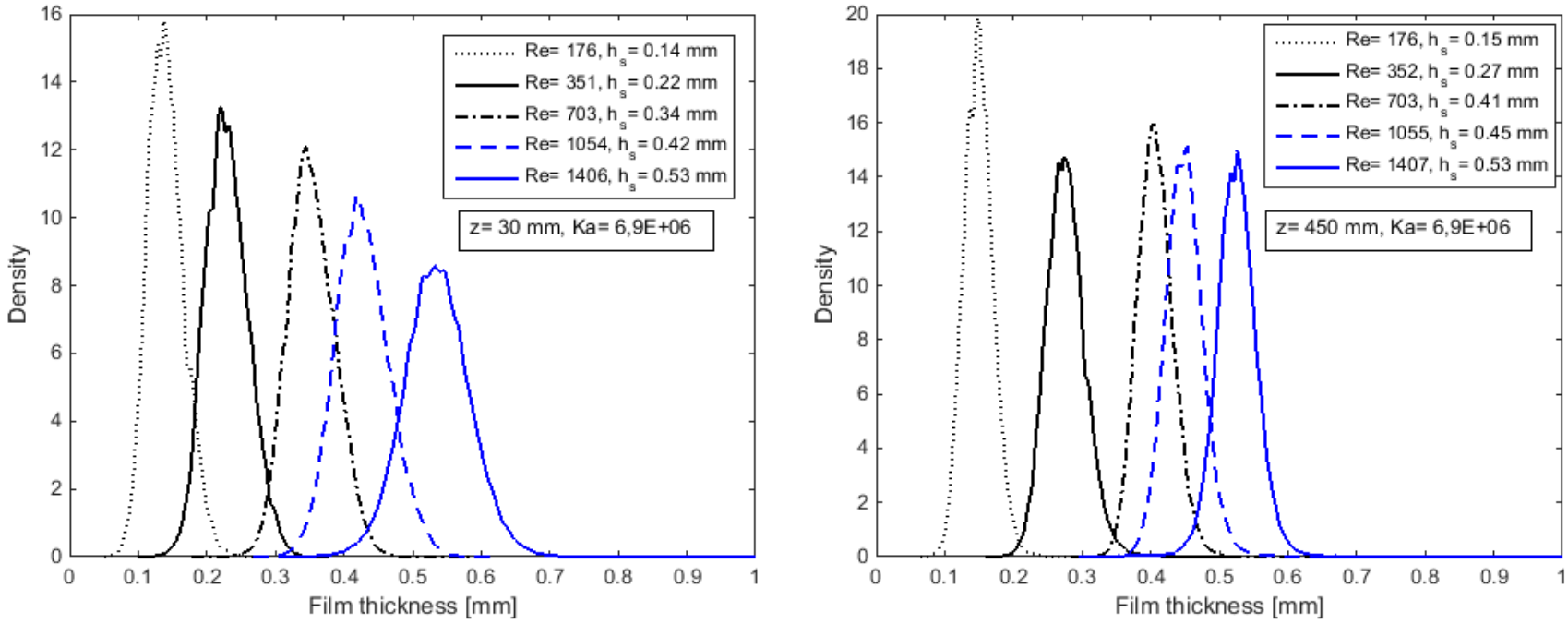

Figure 11.7: PDF at 30 mm (left) and 450 mm right for, $Ka \cong 1{,}6 \cdot 10^9$ *for volume flows 50 l/h-400l/h*

11.7 Film thickness trace – Decay in wave crest at 450 mm

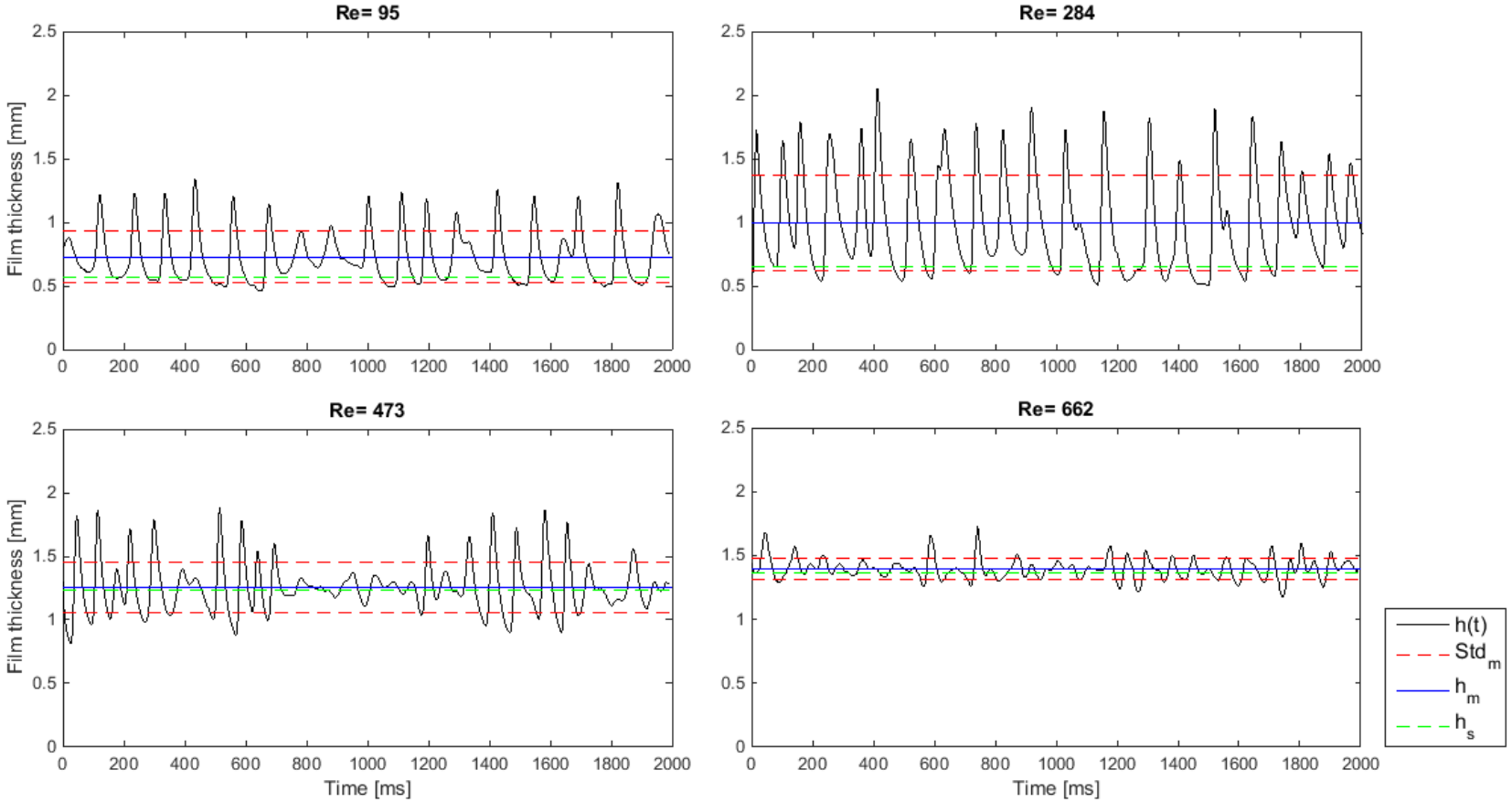

Figure 11.8: Film thickness trace at 450 mm for $Ka \cong 6{,}9 \cdot 10^6$ *showing the decay in wave crest*

11.8 Film thickness trace – Transition to turbulence at 4500 mm

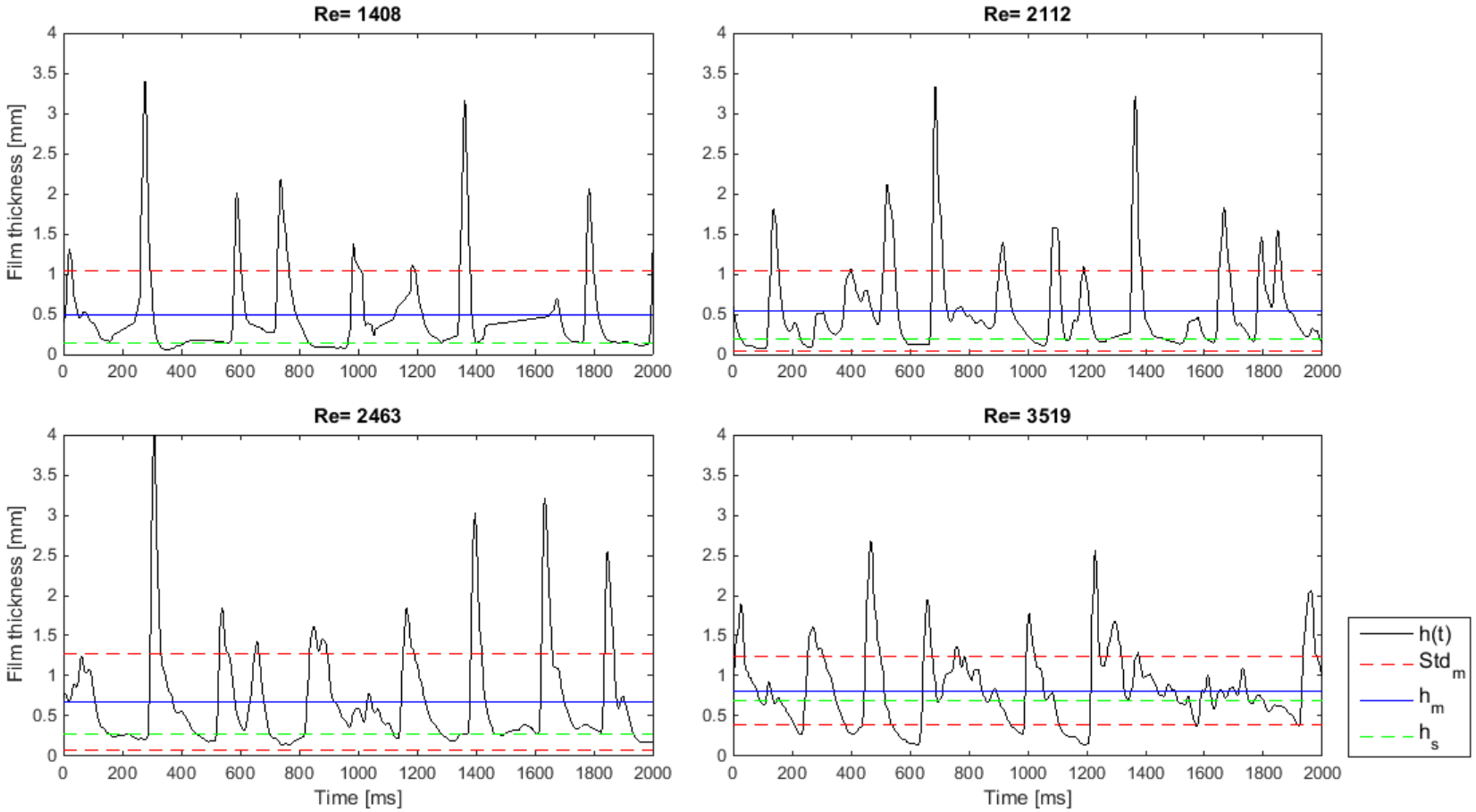

Figure 11.9: Film thickness trace at 4500 mm for $Ka \cong 1{,}6 \cdot 10^9$ *showing decay in wave crest, transition to fully turbulent flow regime*

11.9 Validation of measurement

In the following two figures the PDF of different repetition measurements used for validation of the laser device are shown. *Figure 11.10* presents the results for $\overline{Ka} \cong 1{,}6 \cdot 10^9$ at all for positions whereas *Figure 11.11* shows the results for $\overline{Ka} \cong 6{,}9 \cdot 10^6$. The PDF is used as it shows the frequency of all film thickness values arising. Thus this is better than by only comparing a single value as for example the mean film thickness. The solid lines represent the first measurement, whereas the dotted lines represent the repititions.

In total it can be said that the results of the laser measurement are valid. The differences of the substrate thickness h_s are mostly within the accuracy of 0,1 mm the laser can measure, determined during the calibration process. Only two repetitions in *Figure 11.11* b) and c) differs significantly. In b) vibrations could be observed influencing the result. The reason for the higher deviation c) has not been observed but may be related also to vibrations.

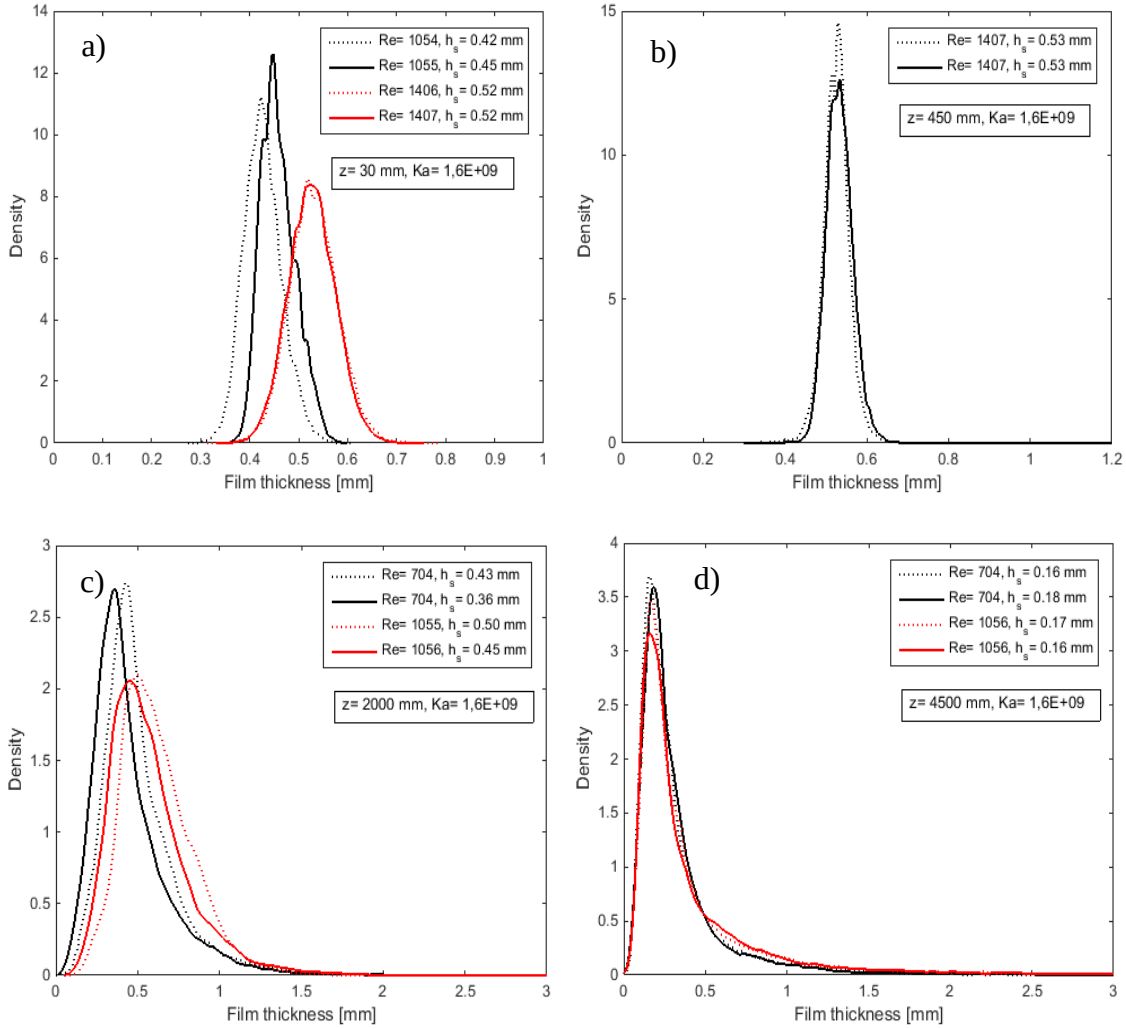

Figure 11.10: PDF used for the validation of the laser measurement results for $\overline{Ka} \cong 1{,}6 \cdot 10^9$ *at a) 30 mm b) 450 mm, c) 2 m and d) 4,5 m*

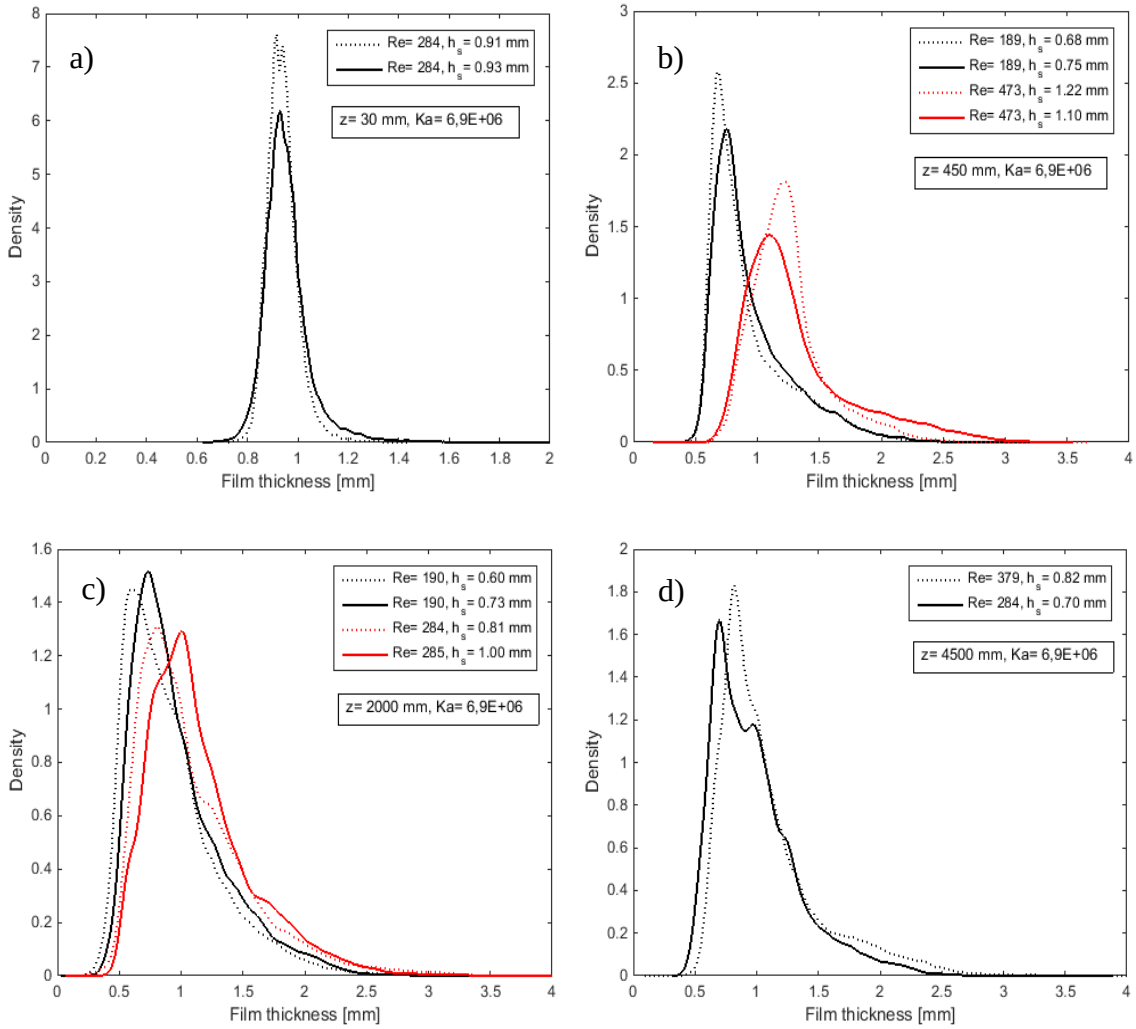

Figure 11.11: PDF used for the validation of the laser measurement results for $\overline{Ka} \cong 6{,}9 \cdot 10^6$ *at a) 30 mm b) 450 mm, c) 2 m and d) 4,5 m*